

Review

Open Access



Recent advances in shape selectivity of MFI zeolite and its effect on the catalytic performance

Lan Zhang, Ning Liu, Chengna Dai, Ruinian Xu, Gangqiang Yu, Biaohua Chen, Ning Wang*

Faculty of Environment and Life, Beijing University of Technology, Beijing 100124, China.

*Correspondence to: Prof. Ning Wang, Faculty of Environment and Life, Beijing University of Technology, Ping Le Yuan 100, Beijing 100124, China. E-mail: ning.wang.1@bjut.edu.cn

How to cite this article: Zhang L, Liu N, Dai C, Xu R, Yu G, Chen B, Wang N. Recent advances in shape selectivity of MFI zeolite and its effect on the catalytic performance. *Chem Synth* 2022;3:2. <https://dx.doi.org/10.20517/cs.2022.31>

Received: 12 Oct 2022 **First Decision:** 16 Nov 2022 **Revised:** 3 Dec 2022 **Accepted:** 16 Dec 2022 **Published:** 1 Jan 2023

Academic Editors: Jun Xu, Bao-Lian Su **Copy Editor:** Ying Han **Production Editor:** Ying Han

Abstract

MFI zeolite characterized by uniform pore size, adjustable acidity, and high-temperature resistance has a broad application prospect in catalytic reactions. However, controlling the product distribution of zeolite as a catalyst is still confronting great challenges and applications. It is considered as an effective way to control the product distribution by developing and improving new zeolites to modulate their shape selective effect. In recent years, researchers have achieved remarkable successes in investigating the shape selective modulation of zeolites on catalytic reaction and molecular diffusion. The microporous channels of MFI zeolite are the main places for the entry and exit of reactants or product molecules. This review provides the research progress of the shape-selective modulation of MFI zeolite channels and its influence on a series of catalytic performances in recent years. The shape-selective modulation of microporous channels of zeolite, encapsulation of micropores to metals, catalysis of mesoporous zeolite, and the distribution of framework Al were all systematically discussed. The development of advanced catalysts still faces great challenges and potential applications. Finally, we discussed the problems to be addressed urgently in the field of zeolite catalysts in the future.

Keywords: MFI zeolite, straight channels, sinusoidal channels, shape-selective effect

INTRODUCTION

ZSM-5 zeolite has been extensively used in catalysis, such as methanol to aromatics (MTA), methanol to olefins (MTO), isomerization, alkylation and other reaction due to its shape selective effect^[1-5]. It is well-



© The Author(s) 2022. **Open Access** This article is licensed under a Creative Commons Attribution 4.0 International License (<https://creativecommons.org/licenses/by/4.0/>), which permits unrestricted use, sharing, adaptation, distribution and reproduction in any medium or format, for any purpose, even commercially, as long as you give appropriate credit to the original author(s) and the source, provide a link to the Creative Commons license, and indicate if changes were made.



known that ZSM-5 zeolite (MFI topology) consists of two-dimensional sinusoidal channels ($5.1 \times 5.5 \text{ \AA}$) and one-dimensional straight channels ($5.3 \times 5.6 \text{ \AA}$), including two 10-membered rings (10-MR) micropore structure. The straight channels follow the direction of the b-axis with exposed [010] facets, while sinusoidal channels are parallel to the a-axis with exposed [100] and [101] facets^[6]. The critical dimensions at the intersection of the straight and sinusoidal channels are close to 0.9 nm, which is probably the place where the catalytic active sites are located^[7]. The structure diagram of ZSM-5 zeolite is shown in Figure 1, clearly presenting the straight channels, sinusoidal channels, and intersection channels models. The diffusion of guest molecules is closely linked to the channel structure of the host zeolite. Due to the different space limitations of the two channels, the diffusion level is different in the reaction process. Small molecules diffuse readily in sinusoidal and straight channels, while large molecules with diameters similar to those of sinusoidal channels tend to diffuse in straight channels^[8,9]. ZSM-5 zeolite has been extensively applied in C1 catalytic conversion. For example, ZSM-5 zeolite mainly promotes methanol/dimethyl ether (MeOH/DME) polymerization, cyclization, and aromatization to produce aromatics and gasoline in MTA or MTO reactions. In addition, ZSM-5 zeolite is a vital part of bifunctional catalysts in CO₂/CO conversion^[10-14].

It is essential to investigate how to make full use of shape selective effect of ZSM-5. ZSM-5 was applied to the dealkylation of 4-n-propylphenol (4-n-PP). The selectivity of 4-n-PP to phenol and propylene reached 95%. The exceptional selectivity of ZSM-5 is attributed to the shape selectivity of the microporous channels, avoiding disproportionation/transalkylation caused by a transition state shape selectivity^[15]. However, due to the pore size limitation of ZSM-5 zeolite, low-value C₁₀ aromatics as solvent and transmethylation-agentia cannot enter the zeolite, resulting in almost no transmethylation reaction in the zeolite micropores in the methylation of 2-methylnaphthalene to 2,6-dimethylnaphthalene^[16]. By precisely adjusting the size and morphology of ZSM-5 single crystal, researchers tuned the length of microporous channels, and the external specific surface area, and enhanced the diffusion performance of guest molecules in microporous channels^[17-19]. Zeolites with small crystal sizes have larger external area and higher intracrystalline diffusion rate, which exhibit superior performance in improving the utilization rate of catalyst, reducing deep reaction, and coking deactivation. Many studies have indicated that the shortening of b-axis in the ZSM-5 single crystal enhances the diffusion rate of guest molecules, hence improving the stability of ZSM-5 and reducing the probability of microporous channel blockage, while the shape selectivity of zeolites is reduced^[18]. The extended b-axis (thicker layers) with a longer diffusion can lengthen the reaction path and thus contribute to the shape selectivity of aromatics, but it was easy to form polycyclic aromatics, and the stability was decreased^[20].

In many carbon-based catalytic reactions, coke formation is one of the main reasons for the deactivation of ZSM-5 zeolite catalysts due to the limitation of microporous channels. To enhance the coke resistance of ZSM-5, it is a favorable method to fabricate mesopores on zeolite^[10,21,22]. The hierarchical structure of ZSM-5 facilitates the diffusion of reactants and intermediate species, greatly shortens the molecular diffusion distance, and enhances the coke resistance of zeolite. The hierarchical pore structure of ZSM-5 still exerts a vital role in improving the selectivity of products. Mesoporous ZSM-5 displays catalytic performances with a two-fold p-xylene (PX) yield compared with ordinary ZSM-5 in the isomerization of o-xylene (OX)^[23]. Kang *et al.* the Ru-based mesoporous ZSM-5 catalyst with high selectivity for the production of C5-C11 isoparaffins from syngas^[24]. The selectivity of isoparaffins is as high as 80%. This is mainly due to the hierarchical porous structure and unique acidity of zeolite plays an important role in the excellent selectivity^[24].

The adjustable acid sites and active sites in the zeolite framework also play a critical role in the catalytic reaction. The acid sites of MFI zeolite mainly originate from the isomorphous substitution of Al for Si at

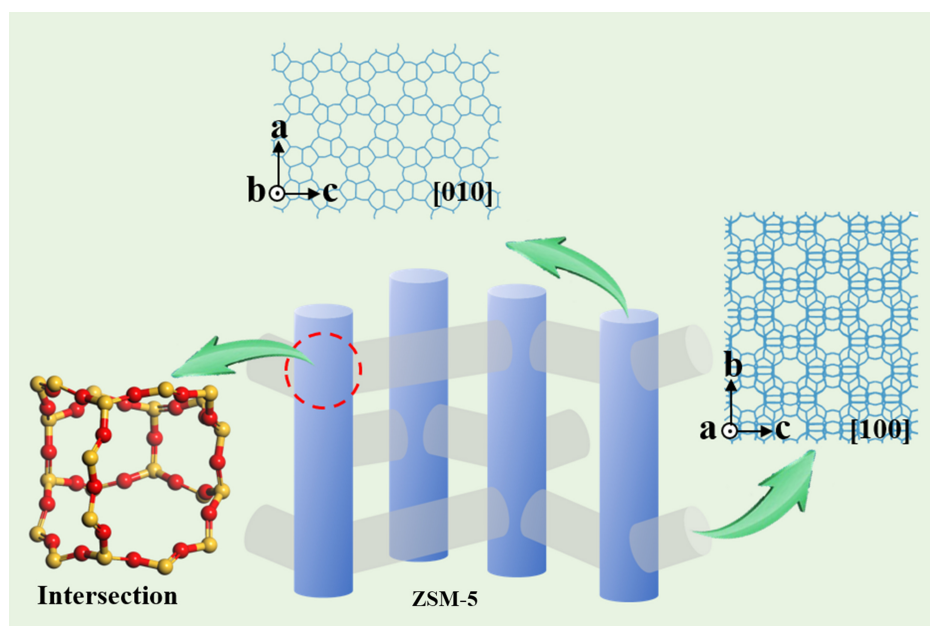


Figure 1. Schematic diagram of straight channels, sinusoidal channels and intersection channels in ZSM-5 zeolite.

different zeolite frameworks^[25]. The location of Al in the zeolite framework was influenced by the synthesis temperature and the pH of the solution. Therefore, the changes in the location of Al or the distribution of acid sites in zeolite framework can change the environment of active acid center and the shape selectivity of pore channels^[26]. Wang *et al.* shows that the aromatic cycle and aromatization process preferentially occur at the acid sites in the intersection cavities in the MTO reaction^[27]. The formation of polymethylbenzenes is significantly inhibited at the acid sites in the straight channels and the sinusoidal channels, while the olefin cycle can occur at the acid sites of the straight channels, sinusoidal channels and the intersection cavities^[27]. Meanwhile, the location of active sites exerts a significant impact on a series of catalytic reactions. When the active site is located on the outer surface of the zeolite, it is not difficult to aggregate into large particles under reaction or high temperature conditions. Therefore, to improve the performance of zeolite catalysts, researchers introduced active metals into the microporous channels of zeolite. The active metals in zeolite pores are characterized by small size and uniform dispersion, and remain stable under reaction and high temperature conditions^[28-30].

Therefore, the effective use of ZSM-5 unique channels structure, adjustable acidity and active site to improve the catalytic conversion, product selectivity as well as long-time stability has become the ultimate goal of many researchers. The research progress of the shape-selectivity of MFI zeolite channels and its influence on a series of catalytic performances in recent years were reviewed.

MICROPOROUS CHANNELS

Modulation of straight and sinusoidal channels

The diffusion of guest molecules in the zeolite micropore channels is influenced by numerous factors, including the dynamic diameter of guest molecules, molecular polarity, zeolite size, and the length of the zeolite channels. The differences in pore size and local environment can lead to different adsorption properties of the two types of channels, which will affect the catalytic process and product distribution. It was found that the diffusion coefficients of the straight channels of ZSM-5 zeolite were one order of magnitude higher than those of the sinusoidal channels^[8]. Many studies have shown that furfuryl alcohol, as

an important intermediate species in MTA reaction, had a higher diffusion rate in the straight channels than in the sinusoidal channels^[31-33]. It is considered that olefin cracking occurs at the acid site at the intersection of straight and sinusoidal channels^[9]. The short-chain 2-butene diffuses along the straight and sinusoidal channels of ZSM-5, while the long-chain 2-octene diffuses along the straight channels. The diffusion paths of guest molecules with different kinetic diameters in the microporous channels of ZSM-5 zeolite show the difference. BTX appears to diffuse isotropically. For zeolite crystals with an average diameter of above 5 μm , zeolite channels have a significant impact on the transport of molecules as the aspect ratio of aromatic molecules increases, resulting in anisotropic diffusion of toluene and PX^[34]. This is mainly ascribed to the fact that the importance of intracrystalline diffusion increases with the increase in zeolite particle size, which may indispensably lead to the elevated anisotropic diffusion in zeolite crystals. The kinetic diameter of benzene is smaller than those of the straight channels and sinusoidal channels of ZSM-5 zeolite; thus, benzene, toluene and PX diffuse freely in the two microporous channels of zeolite, and are capable of switching between two microporous channels without major hindrances. The transport of OX and m-xylene (MX) in zeolite micropores is limited^[35]. Perpendicular rotations of PX along the (100) plane are difficult, since the length of PX (0.99 nm) exceeds the maximum diameter of the intersection channels (0.9 nm). It is difficult for guest molecules with larger dynamic diameter to switch from straight channels to sinusoidal channels, leading to the faster diffusion rate of macromolecules in straight channels. Baumgärtl *et al.* reported the transport of MX and PX mixtures in pure siliceous MFI^[36]. Their study showed that the diffusion of PX in zeolite was mainly through straight channels, and the transportation of PX through straight channel openings was about 8 times greater than that through sinusoidal channel openings. The location of MX has a significant effect on the diffusion rate of PX on zeolite. When MX is distributed inside the zeolite, it has a little effect on the diffusion of PX. By contrast, when MX is distributed on the outer surface of zeolite, the diffusion rate of PX decreases significantly. This is possibly because the transportation of PX is mainly carried out through straight channels. When MX is distributed on the outer surface of zeolite, the openings of zeolite channels are hindered, inducing the limited transportation of PX^[36]. DeLuca *et al.* calculated the self-diffusivities of C₆-C₁₂ molecules by the density functional theory (DFT), and found that small aromatic molecules (including benzene, toluene and PX) reasonably diffused through both channels, but the diffusion was faster through straight channels whereas slower through sinusoidal channels^[35]. The large aromatic molecules (including OX, MX and 1, 2, 3-trimethylbenzene) can only diffuse through straight channels, while they have a high diffusion barrier and a slow diffusion rate. The larger aromatic molecules (e.g., 1, 3, 5-trimethylbenzene, pentamethylbenzene) can only exist in the intersections of MFI^[35].

The geometrical structure of the zeolite channels determines the migration and movement behavior of molecules, causing the anisotropy of diffusion^[37]. Figure 2A shows diffusion patterns of three representative trajectories motion types, namely, immobile (a), hybrid (b) and mobile (c) motion. Figure 2B presents the trajectory distribution space of different motion types, indicating that diffusion heterogeneity is random on samples. It is shown that compared with those in sinusoidal channels, there are fewer immobile trajectories in straight channels. By calculating the effective diffusivity in different channels, it is shown that the diffusion rate in the straight channels ($3.10 \pm 0.21 \times 10^{-15} \text{ m}^2 \text{ s}^{-1}$) is 10 times faster than that in the sinusoidal channels ($0.27 \pm 0.10 \times 10^{-15} \text{ m}^2 \text{ s}^{-1}$). When the mesoporous is introduced into ZSM-5 zeolite [Figure 2C], it is found that the immobile trajectory in the straight channels increases while the immobile motion type in the sinusoidal channels decreases [Figure 2D]. In comparison with that of parent zeolite, the effective diffusion constant of sinusoidal channels is increased by one order of magnitude, while that of straight channels is slightly decreased [Figure 2E]^[32]. This indicates that the diffusion ability in sinusoidal channels can be effectively improved while increasing the mesoporous structure of ZSM-5 zeolite, aiming to alleviate the diffusion limit of microporous molecular sieve.

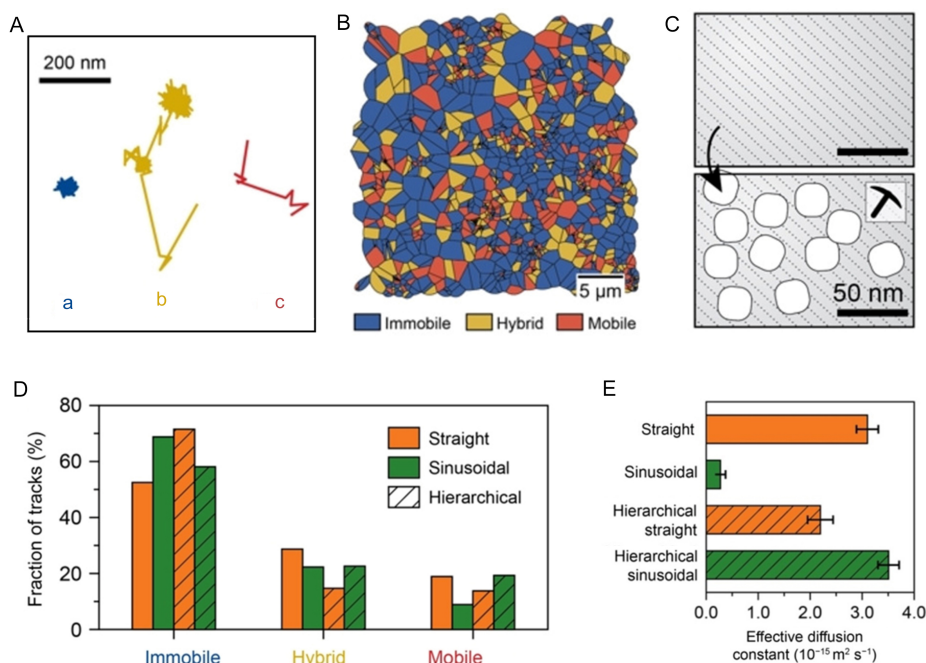


Figure 2. (A) Diffusion patterns of three representative trajectories with a: immobile, b: hybrid and c: mobile motion types. (B) Spatial map of the distribution of trajectories with different motion types. (C) Schematic representation of the introduction of secondary pore networks into zeolites. (D) The fraction of each type of trajectory within the straight (orange) and sinusoidal (green) zeolite channels with secondary porosity (hatched bars), in comparison with the corresponding parent zeolite channels. (E) The effective diffusion coefficients for the straight (orange) and sinusoidal (green) zeolite channels with secondary porosity (hatched bars), in comparison with the corresponding parent zeolite channels. The figure is used with permission from John Wiley and Sons^[32].

Tuning the selective diffusion and conversion of bridging intermediates between two types of channels is crucial for driving tandem reactions over multi-component catalysts. Liu *et al.* prepared the Cr_2O_3 oriented distributed catalysts by extrusion and recrystallization of the physical mixture containing Cr_2O_3 and ZSM-5^[38]. The directional distribution of Cr_2O_3 on the (100) and (101) planes of ZSM-5 induced the high exposure of the (010) plane [Figure 3A]. In the syngas to aromatics (STA) reaction, the C_1^* intermediate species first generated by CO hydrogenation was directly diffused through sinusoidal channels on the (100) and (101) planes of adjacent ZSM-5. Besides, the C_1^* intermediate species was hydrogenated, condensed and aromatized at the acidic site of ZSM-5 to produce aromatics, which then diffused out from the b-axis channels. However, when Cr_2O_3 was non-directed, the intermediate species dispersed randomly, which seriously reduced the orderliness of zeolite channel diffusion [Figure 3B]. The catalyst with the directional distribution of metal oxides can effectively regulate the directional dispersion of products bridging intermediate species; therefore, the CO conversion and aromatic selectivity are greatly improved in STA reaction^[38].

Effect of straight channels length on catalytic performance

In MTA, alkylation and other reactions, b/a-axis length also has a significant influence on the product. Numerous methods have been reported for synthesizing ZSM-5 single crystal with different b-axis lengths, including nanosheet (< 10 nm)^[39-42], 50 nm^[19,43], 100 nm^[18,19], and micrometer-size^[17,44]. Because the diffusion of guest molecules through straight channels is faster than that through sinusoidal channels, the shorter b-axis of ZSM-5 zeolite is more beneficial for the diffusion of reactant and product molecules. ZSM-5 zeolites with different b-axis lengths have been applied in furfural condensation, glycerol dehydration, MTA and numerous other catalytic reactions^[31-33]. In MTA reaction, Zn/ZSM-5 with b-axis (~50 nm) has a higher

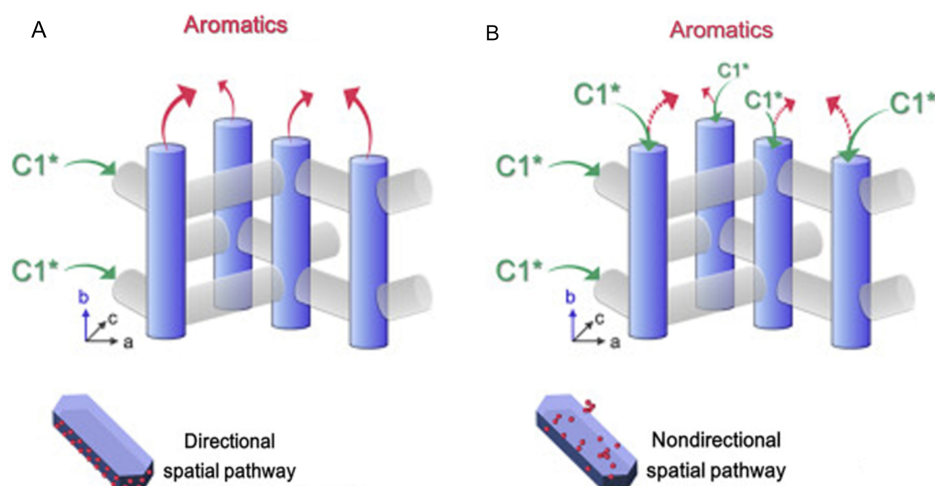


Figure 3. Schematic diagram of Cr_2O_3 distribution on ZSM-5 and directional (A), nondirectional (B) spatial pathway of aromatics generation of intermediate species C1^* in ZSM-5 zeolite channels. The figure is used with permission from Elsevier^[38].

aromatic selectivity (98%), which can be ascribed to its shorter straight channel length. However, with the increase in reaction time, a large amount of carbon deposition is inevitable^[45]. Zhang *et al.* accurately tuned the b-axis thickness of ZSM-5 at 25–100 nm by adjusting the amount and aging time of silicalite-1 seed suspension in the fluoride medium^[19]. This is mainly because that F^- tends to adsorb onto the (010) crystal plane of ZSM-5 in the nearly neutral seed suspension and deposit into the directional growth of zeolite b-axis. The n-heptane cracking catalyst is prone to deactivation because of the carbon deposition-induced channel blockage. The short b-axis zeolite is beneficial for increasing carbon capacity and promoting heptane cracking reaction^[19].

Kim *et al.* dispersed Pt on MFI (ZSM-5) zeolites with various crystal thicknesses ranging from 2 to 300 nm by ion exchange^[46]. It was found that the low isoheptane selectivity of bulk zeolite in n-heptane hydroisomerization might be attributed to the diffusion limitation of branched isomers and the consecutive reaction to cracked products. Reducing the thickness of zeolite crystals significantly improves the product selectivity to branched isomers. The increased selectivity can be attributable to the short diffusion path length, making the branching products escape before cracking. Ma *et al.* also suggested that ZSM-5 nanocrystals with short b-axis length exhibited higher activity in MTA reaction^[47]. In the glycerol dehydration to acrolein reaction, the length of b-axis channels significantly affects acrolein selectivity and glycerol conversion. Typically, the ZSM-5 with short b-axis shows the highest catalytic activity, acrolein selectivity (88%) and stability, which can be associated with its good proximity to the active site in micropores and short diffusion channels. The long b-axis may easily lead to catalyst coking and deactivation^[18]. In addition, Wang *et al.* found that in the Zn/ZSM-5 catalysts with similar a-axis length, acidity and porosity, the b-axis length (2–220 nm) had an obvious impact on product diffusion and carbon deposition location during the MTH reaction^[6]. Methylbenzene (MB), a circulating intermediate species in the reaction process, is more likely to diffuse from the 2 nm straight channels to the outer surface for methylation reaction, resulting in the higher aromatic selectivity, while the thicker b-axis (longer straight channels) leads to higher olefins selectivity. In addition, as revealed by analysis of the catalyst after reaction, the carbon deposition in zeolites with short b-axis was mainly distributed on the (010) surface, perpendicular to the straight channel exposure plane, indicating that the product mainly diffused through the straight channels^[6].

The reaction of toluene alkylation or xylene isomerization on ZSM-5 zeolite is related to the length of zeolite b-axis. The intrinsic shape-selectivity ability can be further enhanced if ZSM-5 crystals stack on (010) plane forming one-dimensional oriented assembly along the crystallographic b-axis^[48]. Ma *et al.* reported the synthesis of three-dimensional b-oriented MFI superstructures by vapor treatment of TPAOH-coated amorphous scaffold replicating bacterial cellulose (BC)^[48]. TPA⁺ exerts a vital role in the synthesis process, not only as a structural directing agent (SDA) for zeolite nucleation, but also as a linker to produce b-oriented assembly. BC nanofibers are responsible for the oriented assembly forming three-dimensional b-directional MFI superstructure. The ZSM-5 zeolite shows outstanding selective adsorption for PX over OX^[48]. Liu *et al.* synthesized micro-sized micro-mesoporous ZSM-5 with a cationic amphiphilic copolymer as a mesoporous template, which is more conducive to forming bulky polycyclic compounds^[17]. In addition, to design a micrometer chained ZSM-5 composed of multiple single crystals with the b-axis length of 200 nm, urea and starch were added to the aluminosilicate gel [Figure 4A]. Starch acted as an additive for the formation of mesopores and as a linker for crystals. The surface energy of the (010) plane was the most propitious to the bonding between crystals, which was mainly due to the abundant hydroxyl groups in starch and the dehydration of hydroxyl groups in ZSM-5 crystals to form the chain-like ZSM-5. Long chain-like zeolite is more beneficial for the conversion of MX into PX^[49]. In addition, Wang *et al.* also synthesized the chain-like ZSM-5 with n-octyltrimethoxysilane being the pore-forming and self-assembling agent for CO₂ hydrogenation to aromatics [Figure 4B]^[50]. The TEM image of chained ZSM-5 is shown in Figure 4C. As observed, when ZSM-5 (0.73 μm) was mixed with ZnZrOx, the selectivity for aromatics without CO was above 68%, and the conversion of CO₂ was 17.5% [Figure 4D]. The ZSM-5 with a chain length of 0.73 μm had the highest Brønsted acid sites (BAS) and the largest mesoporous volume. BAS are favorable for the conversion of intermediates to hydrocarbons, and the large pore volume contributes to increasing the mass transfer rate of MeOH/DME from ZnZrOx to ZSM-5 zeolite. However, the increasing chain length (1.41 μm) led to the decreased CO₂ conversion and aromatics selectivity [Figure 4D], possibly because the increased chain length reduced the mass transfer rate in zeolite^[50].

In the research of Liu *et al.*, aromatics distribution was controlled by changing the crystal size of ZSM-5 along the b-axis^[11]. According to their results, the proportion of C₉₊ selectivity in total aromatics was not related to zeolite morphology, but was closely associated with crystal size along the b-axis. There is a linear relationship between “substitution ratio of aromatic ring” (S_{C₉₊}/A) and morphology parameter (1/b) in the relay catalyst consisting of the physical mixture of Cr₂O₃ and ZSM-5 [Figure 4E]. Therefore, the aromatics distribution can be easily controlled by adjusting the crystal size of ZSM-5 along the b-axis. The smaller crystal size of ZSM-5 along the b-axis is better for the formation of C₉₊ aromatic compounds, whereas the larger crystal size of ZSM-5 along the b-axis is more conducive to the formation of benzene, toluene, xylene (BTX) and trimethylbenzene (triMBs)^[11]. Yang *et al.* utilized urea to control the b/a axis length of ZSM-5 and synthesized the ZSM-5 and ZnCrOx composite catalysts under similar acidic and aluminum chemical environments^[51]. Their results showed that although the lower ratio of b/a axis lengths of the crystals resulted in higher aromatics selectivity, it did not affect the selectivity for small molecules such as CH₄ and C₂₋₄. According to their results, straight channels were more conducive to the diffusion of aromatics, while sinusoidal channels inhibited the diffusion of aromatics. The pore sizes of sinusoidal channels and straight channels were much larger than the dynamic diameter of small molecules, and the diffusion of small molecules was almost not restricted by zeolite channels. Therefore, the selectivity for high carbon products could be controlled by adjusting the ratio of two channels^[51,52].

Shape-selective effect of sinusoidal channels

Due to the high investment and high energy consumption in the separation process of the chemical product, it is essential to tune the catalyst to achieve high selectivity for the single product and reduce the cost of chemical separation. PX is highly demanded in bulk chemicals, and it is mainly used in the

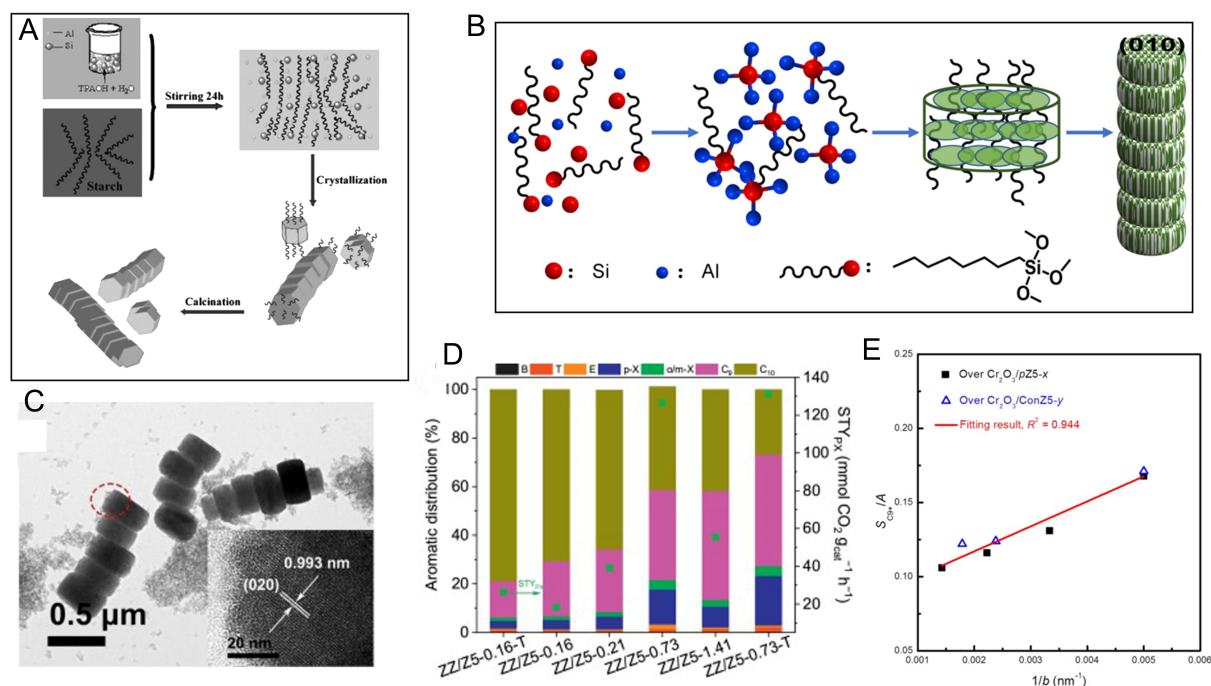


Figure 4. (A) Schematic diagram of ZSM-5 chain synthesis using urea and starch. The figure is used with permission from John Wiley and Sons^[49]. (B) Schematic diagram of ZSM-5 chain synthesis using n-octyltrimethoxysilane. (C) TEM images of the 0.73 μm chained ZSM-5. (D) Catalytic performance of physical mixture of ZSM-5 and ZnZrOX with different chain lengths for CO₂ hydrogenation. Reaction conditions: ZnZrOx (0.5 g) + HZSM-5 (0.5 g), H₂/CO₂/N₂ molar ratio 72/24/4, F = 17 mL min⁻¹, 315 °C, 3.0 MPa, and TOS = 40 h. The figure is used with permission from Elsevier^[50]. (E) Linear fitting between S_{C₉+/A} and 1/b. The figure is used with permission from American Chemistry Society^[11].

production of polyester, film, plastic and other products. Nevertheless, due to the limitation of thermodynamic equilibrium, the isomerized content of PX in xylene is low, and the boiling points of the three isomerization are close (OX: 144.4 °C, MX: 139 °C and PX: 138.4 °C), making it difficult to obtain high-purity PX. Interestingly, the sinusoidal channel size of ZSM-5, which is slightly smaller than the straight pore size, is precisely comparable to the kinetic diameter of PX, while the kinetic diameters of MX and OX are larger than the micropore size. Accordingly, numerous researchers improve the PX selectivity in toluene methanol methylation or MTA reaction by exposing more (100) surfaces^[53,54]. Figure 5A and B show the possible diffusion paths of PX through the straight and sinusoidal channels of ZSM-5 zeolite. By calculating the free energy barriers for the diffusion of MX and PX through the straight and sinusoidal channels, it was found that the free energy barriers for the diffusion of PX via the straight and sinusoidal channels were 19.4 and 15.9 kJ mol⁻¹, respectively [Figure 5C]. The energy barriers of MX diffusion through the straight and sinusoidal channels were 23.2 and 46.8 kJ mol⁻¹, respectively [Figure 5D]. Under the same conditions, the diffusion of PX was always faster than that of MX. The isomerization of PX in HZSM-5 had a higher barrier than diffusion, and thus it tended to diffuse away from zeolite rather than isomerization [Figure 5E]. However, the diffusion barrier of MX through the sinusoidal channels was much higher than its isomerized barrier [Figure 5F]. Therefore, MX in the sinusoidal channels is more likely to be isomerized into PX^[55].

Some researchers modulate the selectivity for catalytic reactions by synthesizing zeolites with different microporous channels exposed. Cai *et al.* discovered that carbon deposition mainly took place on the (100) and (001) planes of ZSM-5^[56]. On this basis, through the pre-deposition of carbon species on these specific planes and the subsequent surface-specific silica deposition, the authors achieved complete coverage of

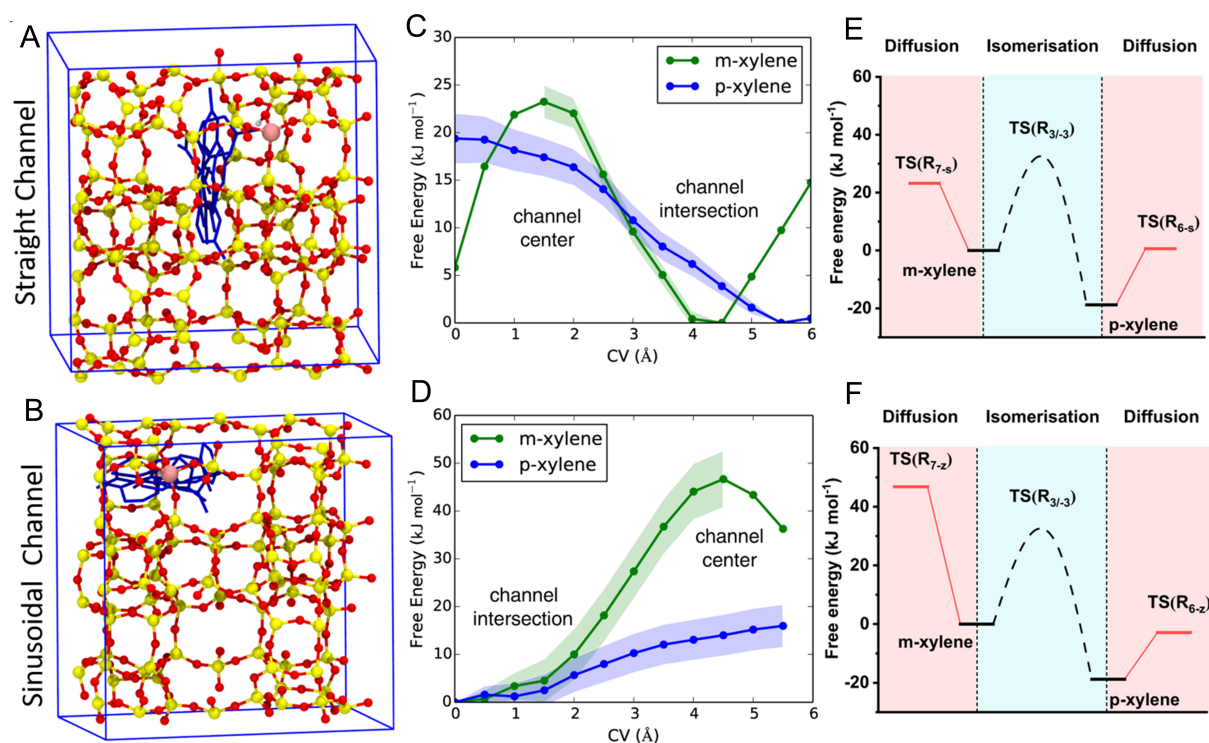


Figure 5. (A) and (B) Possible paths for p-xylene diffusion at the intersection channels. Free energy profiles with a standard deviation of p-xylene and m-xylene diffusing. (C) Along straight channels and (D) along sinusoidal channels obtained from blue-moon simulations. The simplified mechanistic framework of toluene methylation to p-xylene and m-xylene by combing the isomerization and diffusion along (E) straight and (F) sinusoidal channels. The figure is used with permission from Springer Nature^[55].

silica on the (010) plane surface (straight channels). Then, carbon species were removed through calcination, and ZSM-5 zeolites with (100) plane exposure alone were fabricated. The MTO catalytic performance exhibited that the selectivity for aromatics and paraffin was reduced, while that for olefin was greatly improved due to the exposure to a large number of sinusoidal channels^[56]. Besides, Bonilla *et al.* synthesized a leaflet-shaped silicalite-1 crystal and used it as a seed to synthesize MFI zeolite membrane with only the exposure of a-axis^[57-59]. In the silicalite-1 film, the prepared leaflet-shaped crystal was assembled into the a-oriented (a-axis normal to the substrate plane) monolayers on appropriate substrates. Lai prepared ZSM-5 with small membrane thickness (approximately 1 μm) and preferential orientation of straight channels through the membrane^[59]. The excellent zeolite makes the transport of p-xylene faster and is propitious to the separation of PX and OX. The MFI zeolite membrane showed high selectivity for PX during xylene separation^[57,58,60,61]. Wang *et al.* synthesized twin ZSM-5 with intergrowth structure, covering the (100) plane on the (010) plane of the coffin-shaped ZSM-5 [Figure 6A]^[53]. With the increase in temperature, the sizes of sinusoidal channels and straight channels of ZSM-5 decreased slightly [Figure 6B]. The twin ZSM-5 zeolite mainly exposed the (100) plane, and the number of sinusoidal channel openings was as high as 73%, while that of sinusoidal channel openings for the coffin-shaped ZSM-5 with unobstructed straight channels was only around 43%. The coffin-shaped ZSM-5 was more likely to adsorb m-xylene than twin ZSM-5, indicating the effectiveness of this intergrowth structure on distinguishing xylene isomers. The slight change in size led to a high selectivity for PX (> 99%) of twin ZSM-5 and extremely stable catalytic performance (> 220 h) during the alkylation of methanol with toluene [Figure 6C]. Moreover, Miao *et al.* also applied the twin ZSM-5 with the above highly exposed (100) plane in loading Mo species for the xylene isomerization reaction^[54]. There were strong acid sites on the outer surface of intergrowth ZSM-5, and ethylbenzene was dealkylated in the zeolite channels, which improved

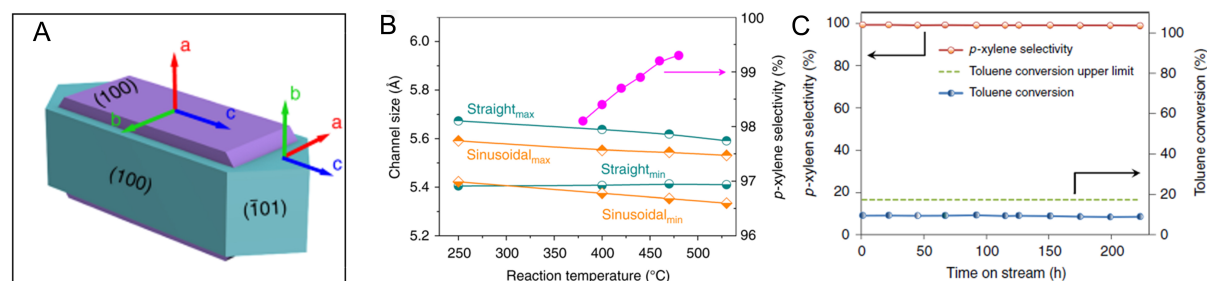


Figure 6. (A) Model of twin ZSM-5 crystals. (B) Effects of reaction temperature on ZSM-5 shape selectivity to p-xylene, and on ZSM-5 straight channels and sinusoidal channels sizes. (C) Toluene conversion and p-xylene selectivity evolution with time on stream. The figure is used with permission from Springer Nature^[53].

the selectivity for benzene. In the mixed C_8 aromatics reaction, 5% Mo/ZSM-5 exhibited the highest catalytic activity with the ethylbenzene conversion rate of 71.2%, the PX yield of 24.6% and the xylene loss of 1.65% xylene loss^[54]. However, the channel shape selectivity effect of MFI zeolite on generating PX is not perfect. This is mainly because the framework of ZSM-5 zeolite is not a rigid structure, which is affected by the reaction temperature. The breathing vibration of the zeolite framework causes a slight change in the pore size of the zeolite, which may cause slightly larger molecules such as MX to enter the zeolite channel and lower the selectivity of PX^[59].

For shape-selective catalysis, the acid sites on external surfaces show different properties from those of bulk sites and can promote the formation of undesirable products. The aluminum species has been well-known to be enriched outside ZSM-5, while silicon is enriched inside ZSM-5. Generally, acid etching can remove the external Al, whereas alkali can dissolve the internal silicon. NaOH treatment of ZSM-5 crystals is suggested to result in the characteristic hollow coffin-shaped zeolite crystals, where the silicon-rich core is leached and the aluminum-rich rim is preserved. Aluminum zoning can be observed in ZSM-5 crystal, with aluminum preferentially existing on the outer surface. The surface of acid-treated ZSM-5 crystal becomes rough, indicating that acid treatment dissolves aluminum on the zeolite surface^[62]. Surface passivation has been identified as an effective method to improve the product selectivity. Zuo *et al.* reported that deposition of tetraethyl orthosilicate (TEOS) on the surface of ZSM-5 zeolite formed a layer of inert silicalite-1, which blocked the external acid site of zeolite, thus improving the selectivity for PX in the methylation of toluene to PX^[63]. With the increase of deposition times, TEOS would block the micropores of ZSM-5 and hinder the diffusion of molecules, causing the alkylation of PX into 4-ethyltoluene and triMB by-products^[63]. Since the deposition method causes pore blockage and substantially increases the diffusion resistance, a strategy to address the aforementioned drawbacks of zeolite passivation is the epitaxial growth of a silicalite-1 (S1) shell on the core zeolite crystallites. Zhang *et al.* designed the Cr/Zn+Zn/(Z5@S1) relay catalyst that efficiently converted syngas into PX in one step^[64]. Notably, S1 in the special Zn/(Z5@S1) core-shell structure effectively covered the acid sites, thus inhibiting the formation of unnecessary PX isomerization and promoting the directional synthesis of PX. Their results showed that the CO conversion and the xylene selectivity were up to 55.0% and 77.3%, respectively, and the selectivity for PX in the total product was 27.6%^[64]. Additionally, they also designed the Na-FeMn/(HZSM-5@S1) capsule catalyst using a simple solvent-free method for the direct conversion of CO₂ to aromatics. The PX selectivity in xylene was as high as 81.1%, because the S1 shell effectively regulated the acidity on zeolite surface and inhibited the alkylation and isomerization of PX on zeolite surface^[65]. Using ultra-dilute liquid phase growth technique, Wang *et al.* designed the hollow Zn/MFI single crystal with triple shells^[66]. The obtained composites possessed one ZSM-5 layer (about 30 nm) in the middle and two silicalite-1 layers (around 20 nm) epitaxially grown on both sides of ZSM-5. Zn/(S1@Z5@S1) catalysts exhibited a fairly long lifetime (100% methanol conversion

for more than 40 h) in MTA reactions, and the selectivity for PX/xylene was up to 90%^[66].

CONTROL OF ACTIVE METALS IN ZSM-5 ZEOLITE MICROPOROUS CHANNELS

MFI zeolite with unique microporous structures is a promising support for encapsulating metals, which can effectively control the size and dispersion of metal particles. Utilizing the confinement of narrow 5/6-MRs may be a viable route to immobilize single atoms and pseudo-single atoms composed of several metal atoms^[67,68]. Besides, anchoring metal clusters on ZSM-5 zeolite effectively confines the excessive growth of metal by the interaction of metal clusters as well as the support and spatial limitation of the zeolite framework, aiming to avoid the reduction of catalyst active sites and improve the stability of catalysts^[69,70]. There are numerous methods for the encapsulation of metal within ZSM-5 zeolite, including impregnation method^[71], ion-exchange method^[72,73] and one-pot synthesis method^[28,29,74,75]. Different metal encapsulated methods are shown in Table 1. Among them, the impregnation method is one of the most feasible and common methods used to prepare zeolite-supported metal catalysts in industry. With the wet impregnation method, Au nanoparticles were stably encapsulated in the intracrystalline mesoporous of silicalite-1 zeolite, and the nanoparticles were 2-3 nm in diameter with only a small fraction of the particles being situated on the zeolite surface. The catalyst had high activity and selectivity for gas-phase oxidation of ethanol^[76]. Moreover, Wang *et al.* encapsulated the subnanometric noble metals in the self-pillared MFI zeolite nanosheets by the incipient wetness impregnation method^[71]. The schematic diagram of the synthesis process of Rh-Ru nanoclusters in self-column MFI nanosheets is displayed in Figure 7A. As observed, the Rh, Ru and various Rh_xRu_{1-x} bimetallic clusters were uniformly dispersed within the sinusoidal 5-MRs of MFI and remained stable at high temperatures. The successful encapsulation of these noble metals mainly depends on the specific structure of self-pillared MFI zeolite, which possesses a larger external surface and abundant Si-OH defects compared with the conventional MFI zeolite framework. They are propitious to the dispersion and immobility of metals in the zeolite rings^[71]. However, the impregnation method usually leads to the formation of large metal particles and uneven dispersion, which affects the catalyst activity and stability.

Ion-exchange is a favorable method to introduce metal cluster catalysts into zeolite, which can easily control the number of metal sites^[69,70]. Iida *et al.* introduced Pt²⁺ ions into the Zn-containing MFI (Zn-MFI) zeolite framework through ion exchange to form Pt²⁺/Zn-MFI [Figure 7B]^[72]. After reduction treatment, PtZn_x bimetallic nanoclusters were successfully encapsulated in the micropores of zeolite^[73]. Van den Broek *et al.* prepared the Pt/HZSM-5 catalyst by the ion exchange method, with [Pt(NH₃)₄]²⁺ being a precursor^[73]. After treatment in the oxygen atmosphere, Pt²⁺ was found in the ZSM-5 zeolite. Then, by reduction in the H₂ atmosphere, small Pt particles were formed in the micropores of HZSM-5 zeolite^[72]. Nevertheless, a small amount of metal is introduced into zeolite during the ion exchange process, which usually requires to be washed continuously and repeatedly or even at a high exchange temperature. Moreover, the exchange metal sites on the zeolite outer surface and the solution pH may probably cause the pre-precipitation of metal ions on the zeolite outer surface.

Although the post-treatment method has been widely used to prepare supported catalysts, it can hardly achieve uniform encapsulation of subnanometal clusters into zeolite micropores. *In situ* encapsulation synthesis can implement the encapsulation of subnanometal clusters in zeolite micropores. *In-situ* encapsulation synthesis can encapsulate subnanometal clusters into sinusoidal 5-MRs of zeolite^[67,84]. The *in-situ* hydrothermal synthesis method depends on the mixing of the original gel (for the synthesis of zeolite) with the organic metal ligand. Using [Pd(NH₂CH₂-CH₂NH₂)₂]Cl₂ as a precursor, Wang *et al.* prepared the nanosized silicalite-1 zeolite confined ultra-small Pd cluster catalysts under the direct hydrothermal condition^[74]. The Pd complexes interacted with the zeolite gel and were encapsulated into the zeolite

Table 1. Metal encapsulation by MFI zeolite microporous channels

Synthetic method	Catalysts	Encapsulated channels	Ref.
Impregnation	Rh _{0.8} Ru _{0.2} /SP-ZSM-5-100	10-MRs	[71]
Ion-exchange	PtHZSM-5	10-MRs	[72]
Ion-exchange	PtZn@MFI	10-MRs	[73]
One-pot synthesis	PtZn@MFI	5/6-MRs	[28]
One-pot synthesis	PdMn@S1	5/6-MRs	[29]
Reductive demetallation	Fe@MFI	5/6-MRs	[77]
Reductive demetallation	CuFe@MFI	10-MRs	[77]
Excitation with ultraviolet light	ZnMFI	10-MRs	[78]
Ultrafast <i>in situ</i> encapsulation	Pt/Sn-ZSM-5	10-MRs	[79]
Interzeolite transformations	M(Pt/Ru/Rh)/MFI	10-MRs	[80]
Ionic liquid-assisted	M(Pt/Pd)@MFI	10-MRs or intersection channel	[81]
<i>In situ</i> two stage hydrothermal synthesis	Ru@H-ZSM-5	10-MRs	[82]
Two-step dry gel conversion	Pt@MFI	10-MRs or intersection channel	[83]

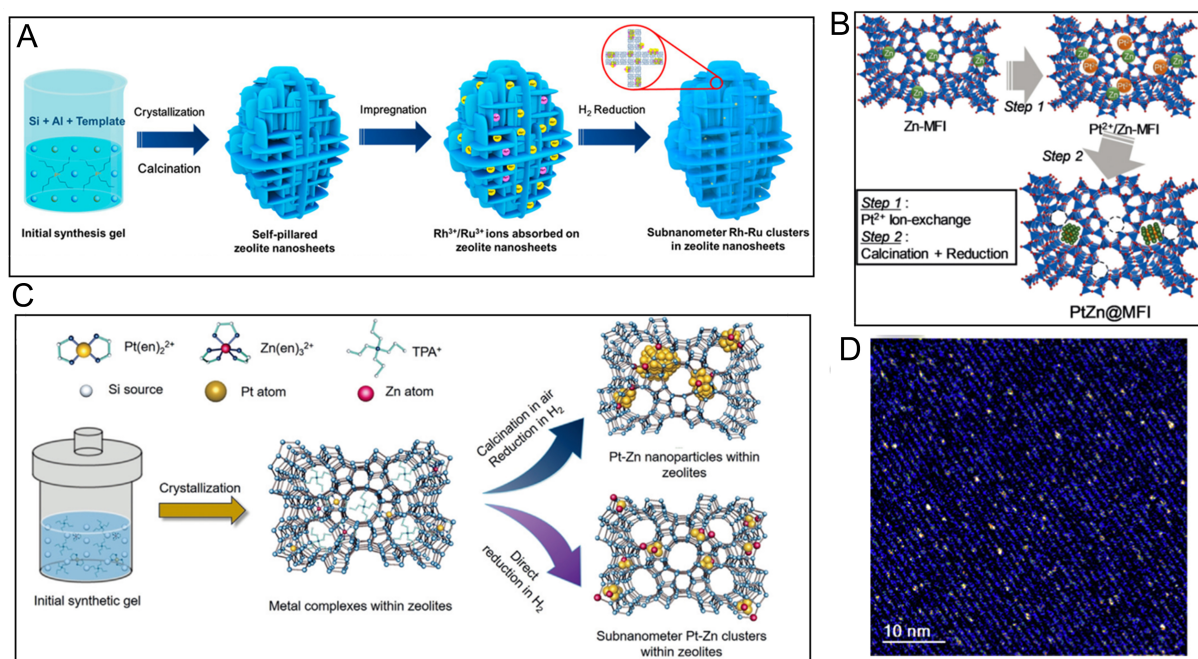


Figure 7. (A) Schematic illustration of the synthetic procedure of subnanometer Rh-Ru clusters in self-pillared MFI nanosheets. The figure is used with permission from American Chemical Society^[71]. (B) Overall schematic of the synthesis route for PtZn@MFI. The figure is used with permission from John Wiley and Sons^[73]. (C) Schematic representation of the synthesis of zeolite-encaged subnanometer Pt-Zn cluster catalysts. The figure is used with permission from John Wiley and Sons^[28]. (D) HR HAADF-STEM image of the K-PtSn@MFI sample along the tilted-[010] direction. The figure is used with permission from Elsevier^[86].

framework by self-assembly during the crystallization process. Upon calcination and reduction, the ultra-small Pd clusters were limited to the intersection of straight channels with sinusoidal channels of MFI zeolite. The catalysts possessed excellent cycle stability in the formic acid decomposition reaction. In addition, Sun *et al.* also develop a ligand-protected direct H₂ reduction method to encapsulate the subnanometer bimetallic Pt-Zn clusters into silicalite-1 zeolite for direct hydrothermal crystallization [Figure 7C]^[28]. The catalyst showed high propylene selectivity (99.3%) and stability in the propane dehydrogenation reaction. The team also synthesized the subnanometric hybrid bimetallic Pd-M(OH)₂

(M = Co, Ni, Mn) clusters within silicalite-1 using a hydrothermal synthesis method^[29,75]. The bimetallic subnanoclusters synthesized by the *in situ* hydrothermal method have an almost unchanged size, and they maintain excellent stability even at high temperatures (700 °C) under the H₂ atmosphere. After adding the second metal species, the Pd ion surface is enriched by electrons and the bimetallic interfacial effect is produced. Moreover, the zeolite with the synergistic effect of bimetallic species exhibits excellent shape-selective catalytic performance and superior thermal stability for the dehydrogenation of formic acid. Sarika also prepared metal clusters (Pt, Ru, Rh) within MFI voids via interzeolite transformation of metal-containing BEA or FAU zeolite through the low temperature hydrothermal synthesis^[80]. Subnanometric clusters instead of nanoparticles were obtained by *in situ* hydrothermal synthesis. This is mainly because the hydrophobic ligand-stabilized metal cationic complexes are closely related to the hydrophobic Si-rich zeolite. As a template, ethylenediamine may influence the regioselectivity distribution of clusters. The formation of subnanometric clusters may also be associated with the relatively mild pH environment in the synthesis process, and the encapsulation of subnanometric clusters only occurs in some pure/high silica zeolites^[30,69].

By using amine-based ligands, Li stabilizes Pd in the microporous channels and voids of nanosized silicalite-1 crystals via the one-pot synthesis method^[85]. The synthesized Pd@S1 catalyst, which has small and highly dispersed encapsulated palladium oxide clusters, exhibits high activity and long-term stability in the complete methane oxidation reaction. Through a one-pot hydrothermal crystallization, Liu *et al.* encapsulated bimetallic Pt-Sn clusters inside the MFI (S1) zeolites using Pt-ethylenediamine complex and SnCl₄ as the precursors^[86]. As observed by high-resolution high-angle annular dark-field scanning transmission electron microscopy [Figure 7D] and integrated differential phase contrast (HR HAADF-STEM and iDPC) imaging techniques, bimetallic PtSn subnanoclusters were preferentially located in sinusoidal channels of silicalite-1 zeolite. Moreover, the introduction of a controllable amount of K⁺ in the synthesis gel compensated for the silanol groups in the zeolite framework and stabilized the subnanometric Pt species, which was beneficial for the dispersion of Pt species. The K-PtSn@MFI catalyst showed outstanding reactivity and stability in propane dehydrogenation reaction. The initial propylene selectivity was as high as 90%, and the propane conversion was close to 70%, which remained even after 65 h on stream^[30,86].

EFFECT OF MESOPOROUS ZSM-5 ON CATALYTIC PERFORMANCE

The hierarchical structure of ZSM-5 facilitates the diffusion of reactants and intermediate species at the acid sites, which also greatly shortens the molecular diffusion distance and enhances the coke resistance of zeolite, thus inhibiting the formation of heavy hydrocarbons and deposition of carbon precursors. Therefore, many researchers have reported the synthesis of hierarchical ZSM-5. The hierarchical structure is mainly synthesized by the template method^[87-91] and the alkali treatment desilication method^[10,21,92-95]. Dong *et al.* reported that amorphous mesoporous SiO₂ spheres were used as silicon source to transform into macroporous zeolite spheres^[95]. At first, the metallic precursors were impregnated on the mesoporous SiO₂ spheres, and one layer of nanocrystalline seed was later coated on the surface of mesoporous SiO₂ spheres by an electrostatic attraction technology, followed by hydrothermal treatment in the TPAOH solution. The external surface of SiO₂ spheres began to dissolve and recrystallize, finally forming silicalite-1^[96]. However, excessive TPAOH or NaOH concentration will lead to excessive etching of ZSM-5 and the formation of nanosheets. With the increase in TPAOH concentration (> 0.3 M), ZSM-5 is etched into sheets^[93,97,98]. The interior of zeolite is preferentially etched in the alkaline solution, while the dissolved Si species migrate to the outer surface for recrystallization. The order of zeolite etching is axis $c > a > b$. Nevertheless, it is found that the recrystallization speed is slower than the etching speed, which results in the formation of four large voids along the direction of [101] and two concave cage nanostructures in the middle of the (100) plane.

Eventually, the (101) and (100) crystal planes are completely etched away, and only a single layer of ZSM-5 exposed (010) plane remains^[93].

To obtain the uniform mesoporous structure, many template agents have been used, including carbon nanoparticles^[99,100], surfactants^[100,101] and polymer beads^[89]. A number of studies have reported that ZSM-5 has an Al-rich exterior and a defective Si-rich interior, and that ZSM-5 is gradually dissolved from the Si-rich interior to the outer surface by alkali treatment with Na₂CO₃^[91], TPAOH^[10,21,92] and NaOH^[93,94]. Therefore, the single crystal forms the hollow ZSM-5. The size and volume of internal void can be adjusted by controlling alkali concentration and pH. Furthermore, the internally dissolved species migrate to the outer surface of ZSM-5 for recrystallization, resulting in the formation of hollow ZSM-5 zeolite^[101]. Then, the hollow zeolite can effectively encapsulate metal compounds through impregnation^[102-105]. The ability of coke resistance of the catalyst is greatly improved. Jin *et al.* used TPAOH or NaOH to form the hollow zeolite^[102]. Due to the stronger alkalinity of NaOH, the zeolite had a thinner outer wall thickness, a larger hollow size and a higher L/B acid ratio, thereby showing higher BTX selectivity in MTA reaction. However, with the increase in reaction time, the active sites responsible for cyclization and hydrogenation in the NaOH-treated ZSM-5 gradually decreased, leading to the reduced aromatics yield. When Na⁺ and TPA⁺ coexisted in the solution, the competitive adsorption of Na⁺ and TPA⁺ occurred, which hindered the interaction between Si-O⁻ and TPA⁺, resulting in the excessive surface dissolution of ZSM-5 and the formation of hollow zeolite with mesoporous surface [Figure 8A]. Interestingly, hollow zeolite with mesoporous surface is more likely to improve the molecular diffusion capacity and the ability of coke resistance. Xu *et al.* reported a yolk@shell FeMn@hollow HZSM-5 nanoreactor used in syngas to aromatics^[10]. The structure was found to have an outstanding spatially and temporally ordered effect, which fully exploited the channel shape selectivity effect of ZSM-5, and played an important role in improving aromatic hydrocarbon yield and coke resistance^[10]. The work of some representative mesoporous MFI encapsulated metals is summarized in Table 2. Moreover, Xu *et al.* also modulated the mesoporous size of zeolite from 7.9 to 20.5 nm by changing Na⁺ concentration, thereby inhibiting the selectivity of C₂₋₄ and improving the selectivity of C₅₋₁₁^[22].

Synthesizing mesoporous MFI zeolite by the long-chain organic surfactant is an insightful method^[116-118]. Choi *et al.* prepared three-dimensional intergrown mesoporous multilayer ZSM-5 nanosheets using the diammonium surfactant [C₂₂H₄₅-N⁺(CH₃)₂-C₆H₁₂-N⁺(CH₃)₂-C₆H₁₃, (C₂₂₋₆₋₆)] as a SDA^[41]. The three-dimensional zeolite consisted of alternating layers of single layer zeolite framework (2 nm thick) and 2.8-nm-thick surfactant micelles (2.8 nm thick). It was because the long-chain bifunctional surfactant guided the simultaneous formation of zeolite at mesoporous and microporous scales. In general, the hydrophobic end of the surfactant leads to the formation of mesoporous zeolite and inhibits the overgrowth of zeolite, while its hydrophilic end results in the formation of ultrathin nanosheets. In methanol to gasoline reaction, an ultra-thin mesoporous structure is beneficial for the diffusion of reaction molecules and product molecules, which can improve the ability of coke resistance, although the mesopore size distribution is rather broad owing to the irregular distortion of zeolite layers. Therefore, Kim *et al.* synthesized the nanosheet zeolite with nanosponge morphologies by using C₂₂₋₆₋₆ as the dual-structure directing agent and bulk MFI zeolite as the seed^[119]. The nanosponge zeolite exhibited a narrow distribution of mesopore diameters (~4 nm). The prepared catalysts had the best catalytic performance in the liquid-phase condensation reactions. Singh *et al.* synthesized the single crystalline mesoporous ZSM-5 with sheetlike mesopores using an amphiphilic template with three diquatery ammonium-terminated alkyl chain branches [Ph-(O-C₁₀H₂₀-N⁺(Me)₂-C₆H₁₂-N⁺(Me)₂-C₆H₁₃·2Br)₃]^[118]. The zeolite formed sheetlike mesopores on a-axis and c-axis and mesoporous ZSM-5 with intercrossed nanosheets along the common c-axis. The authors also synthesized the highly ordered mesostructured MFI zeolite by using [C₆H₅-2N-C₆H₄-

Table 2. Metal encapsulation by MFI zeolite mesoporous channels

Mesoporous synthetic method	Catalysts	Metal size	Mesoporous size	Ref.
Alkaline treatment	Fe ₁ Mn _{0.5} @Z5		~13.8 nm	[10]
Structure-directing	1Pt1Zn/MZ	< 3 nm	~3.3 nm	[106]
Polymer-assisted	Pt@H-ZSM-5	~5 nm		[107]
Steam-assisted recrystallization	Pt@recryst-S1	~10 nm		[108]
<i>In situ</i> mesoporegenfree	Pd@IM-S-1	~2.4 nm	~21.9 nm	[109]
Alkaline treatment	Pt@S-1	~1.3 nm	~30 nm	[110]
Low-temperature hydrothermal synthesis	Pd/MTS-1-in	2.3 nm	3-4 nm	[111]
One-pot method	Pd@mnc-S1	2-5 nm	~30 nm	[112]
One-pot method	Pd@MesoHZSM-5	1-2 nm	~30 nm	[113]
Template method	Rh/C _{PBI} -MMZ-as	1.3 nm	3.5 nm	[114]
One-pot hydrothermal synthesis	Fe ₂ O ₃ @hier-S-1	3-4 nm	5-17 nm	[115]

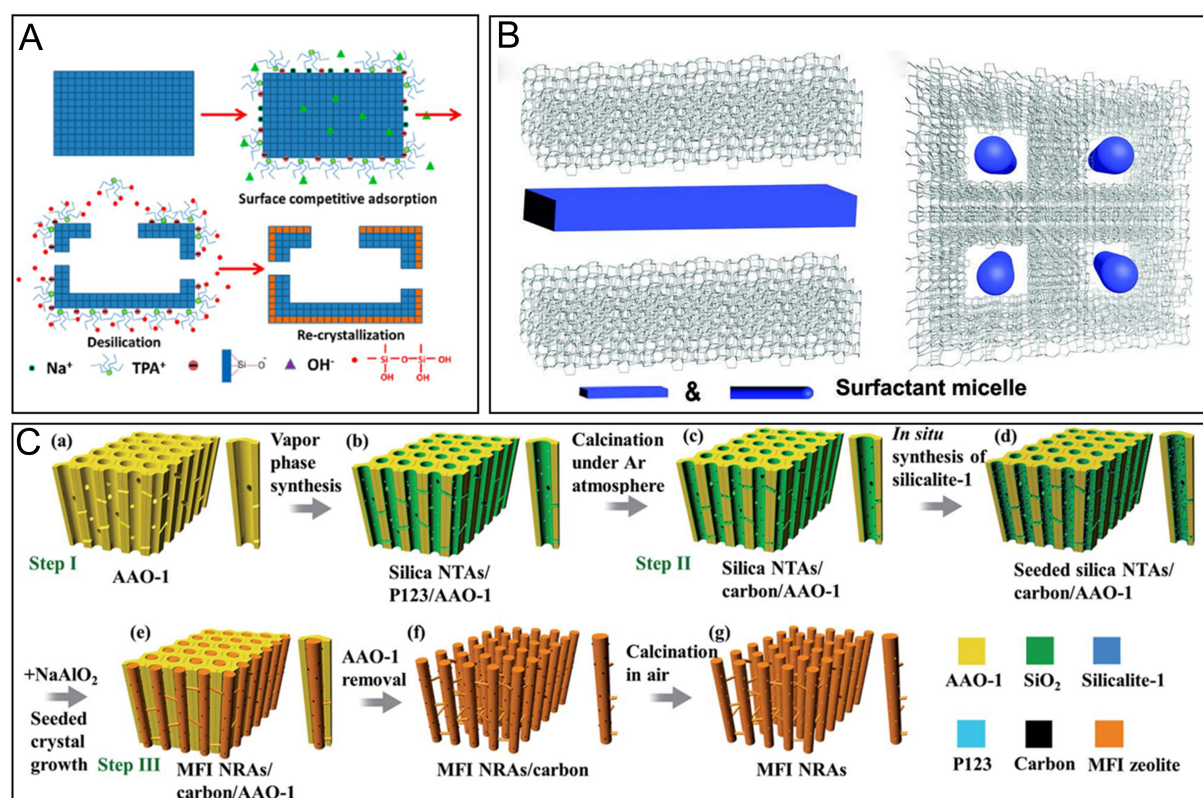


Figure 8. (A) Structure diagram crystallization of MFI nanosheets. The figure is used with permission from American Chemical Society^[101]. (B) Schematic of different mesostructures directed by surfactants with different spatial arrangements (left: a 1D lamellar structure and right: a 2D square cylindrical structure). The figure is used with permission from John Wiley and Sons^[116]. (C) Schematic of the synthetic procedure for nanorod arrays with hierarchically micro-meso-macroporous structure constructed from MFI zeolite crystals by a quasi-solid-state crystallization process. The figure is used with permission from Royal Society of Chemistry^[121].

O-C₁₀H₂₀-N⁺(CH₃)₂-C₆H₁₂-N⁺(CH₃)₂-C₆H₁₃][Br⁻]₂ as a SDA (the SDA by introducing azobenzene into the hydrophobic tail of a surfactant with a diquaternary ammonium head group) [Figure 8B]^[116]. Interestingly, various 2D/3D mesoporous zeolite structures were formed by introducing specific interactions into the hydrophobic part of the surfactant.

Some researchers reported the synthesis of mesoporous self-pillared zeolite nanosheets using relatively inexpensive tetrabutylphosphonium hydroxide as a template. As a SDA, tetrabutylphosphonium hydroxide contributes to the anisotropic growth and 90° rotational intergrowth of MFI framework, while the house-of-card arrangement of nanosheets creates the mesoporous structure^[70,120]. By adopting porous anodic alumina membranes as a rigid scaffold, Wang *et al.* fabricated the unique hierarchically organized MFI zeolite nanorod arrays in a quasi-solid-state system [Figure 8C]^[121]. The micro-meso-macroporous structure of the zeolite was highly interconnected. These MFI showed superior catalytic stability and selectivity for aromatics in MTA reaction.

EFFECT OF Al SITE ON CATALYTIC PERFORMANCE

The acid sites of MFI zeolite are the active centers of catalytic reactions. Therefore, in addition to channel structure, the location and state of acid sites in the channels also directly influence the catalytic activity and product selectivity. The orthogonal MFI contains 12 crystallographical T-sites, while the monoclinic MFI possesses 24 crystallographically different T-sites. At room temperature, the adsorption of small molecules causes a transition from monoclinic crystal to orthogonality^[25]. T₁, T₂, T₃, T₅, T₆, T₇, T₉, and T₁₂ sites are located on the ring at the intersection of straight and sinusoidal channels, T₄ and T₁₀ on sinusoidal channels, and T₈ and T₁₁ on straight channels [Figure 9A and B]^[122,123].

The site of aluminum in the framework will be affected by the synthesis process, such as the Al source, the hydrothermal synthesis temperature and the solution pH. Therefore, it has a direct influence on the catalytic reaction performance^[126]. Liang *et al.* synthesized S-HZ-M and T-HZ-M, with silica sol and TEOS being the silicon sources, respectively^[127]. The two catalysts exhibited similar acidity, morphology and structural properties. However, framework aluminum (Al_F) of S-HZ-M was on sinusoidal and straight channels, while that of T-HZ-M was mainly concentrated at the intersection of sinusoidal and straight channels. Due to the different positions of acid sites, the product distribution in MTO reaction was different between S-HZ-M and T-HZ-M. The acid sites of S-HZ-M were more conducive to the formation of propylene and long-chain olefins, whereas those of T-HZ-M were beneficial for the selectivity of ethylene and aromatics and had a higher hydrogen transfer index. This indicated that sinusoidal and straight channels were conducive to the circulation of olefins, and the channel intersections were less restricted, which was more favorable for the circulation of aromatics. However, when the acid site was located in the channel intersections, pentamethylbenzene (pentaMB) and hexamethylbenzene (hexaMB) carbon pool species were probably formed. Due to the pore size limitation, they were unable to diffuse to the external surface of zeolite, resulting in carbon deposition of zeolite and poor stability of the catalyst^[127]. Kim *et al.* synthesized the hierarchical ZSM-5 by controlling the synthesis temperature and time [Figure 9D]^[124]. Their results showed that low temperatures were favorable for nucleation, while high temperatures were conducive to crystal growth. The temperature difference led to a difference in the site of aluminum. At high temperatures, aluminum site was more likely located at the intersection of sinusoidal and straight channels, while at low temperatures, it was more likely located at straight channels. Therefore, the ZSM-5 zeolite whose acid sites were mainly distributed in the straight channels was more conducive to MTO reaction. Moreover, ZSM-5 zeolite was more propitious to MTA reaction at high temperatures, and its acid sites were mainly distributed at the channel intersection^[124]. Chen *et al.* reported the preparation of [Al, Mg]-ZSM-5 catalysts by the hydrothermal synthesis method^[128]. Mg was successfully introduced into the framework of zeolite and played a good role in regulating the distribution of Al_F. DFT calculation showed that Mg was more likely to replace Si at T₆ site (intersection channels) with the lowest relative energy. Introducing Mg significantly reduced the Al pair content in the intersection channels and increased Al_F level in straight and sinusoidal channels with narrower spaces. Additionally, the yield of light olefins in the catalytic cracking reaction of alkane was improved. This was mainly because the lower aluminum content in the sample and the less Al_F

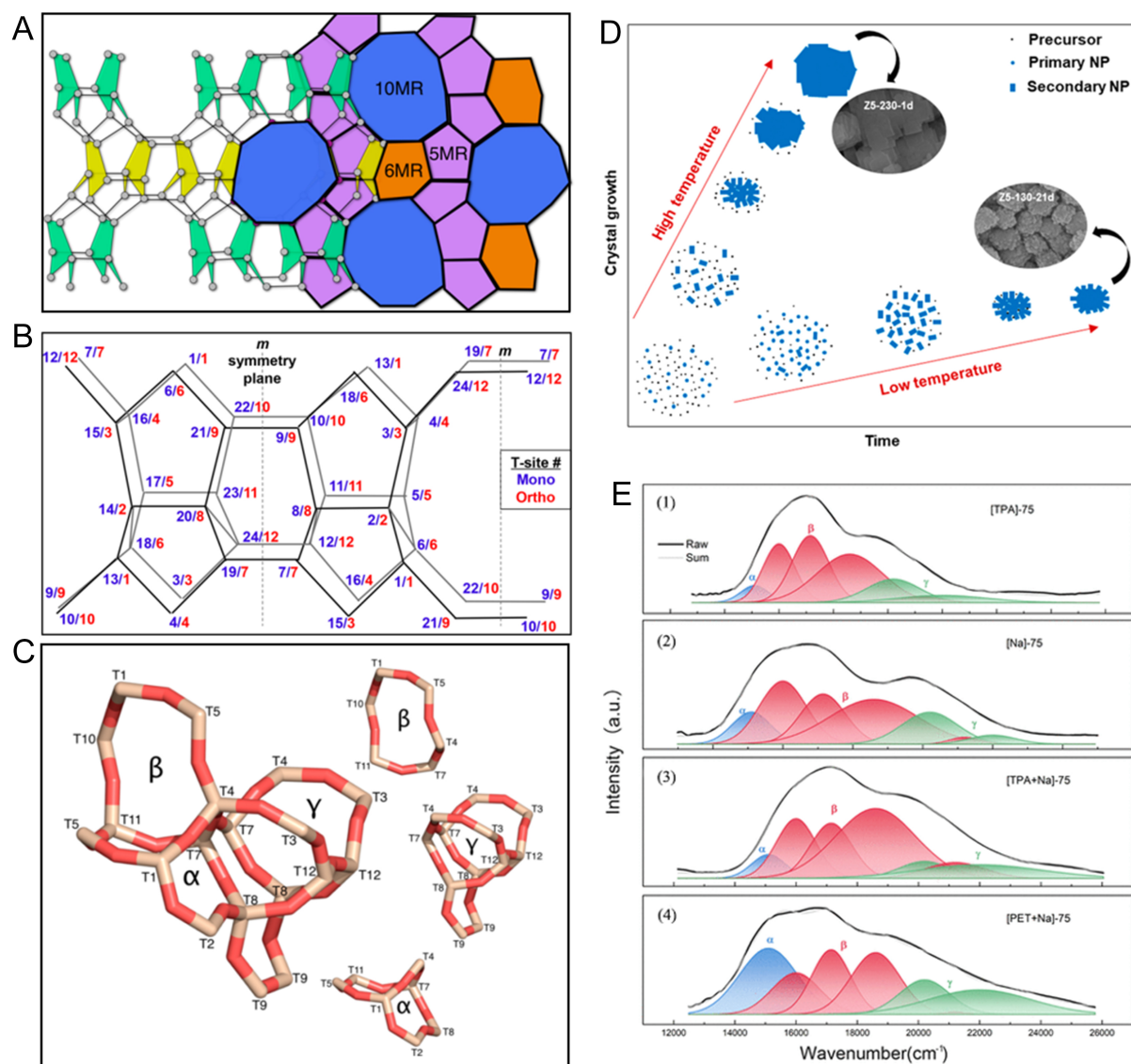


Figure 9. (A) Schematic diagram of ZSM-5 channels. (B) Orthorhombic and monoclinic forms of ZSM-5. The lattice T-sites for the orthorhombic form are shown in red; those for the monoclinic form are shown in blue. (C) Mapping T-sites to α , β , and γ nomenclature. The figure is used with permission from American Chemical Society^[25]. (D) Illustration of crystal growth of ZSM-5 zeolites from primary gel precursor under different hydrothermal synthesis conditions. The figure is used with permission from American Chemical Society^[124]. (E) ^{27}Al MAS NMR spectra of [TPA]-75, [Na]-75, [TPA + Na]-75, and [PET + Na]-75 samples. The figure is used with permission from American Chemical Society^[125].

distribution at the intersection channels effectively inhibited the hydride transfer process in the catalytic cracking reaction^[128].

Different pore-filling agents and organic structure-directing agents (OSDAs) can also control Al_T distribution in ZSM-5 channels. TPAOH and pentaerythritol (PET) were used as the OSDA and pore-filling agent, respectively, and Co(II) UV-vis-DRS peaks were used to analyze Al T-sites [α represents Co(II) adsorbed through straight channels, β indicates intersection channels, and γ stands for sinusoidal channels] [Figure 9C]. Therefore, Al atoms in ZSM-5 synthesized by TPA^+ were selectively located at the channel intersection, while Al atoms existed in both channel intersection and straight/sinusoidal channels in the co-

occurrence of TPA⁺ and Na⁺. When PET as a pore-filling agent coexisted with Na⁺, the uncharged PET molecules distributed Al atoms around Na⁺ species; thus, Al atoms were preferentially located at straight and sinusoidal channels [Figure 9E]. In the methanol-benzene alkylation reaction, ZSM-5 with aluminum located at the channel intersection and straight/sinusoidal channels adsorbed both reactants simultaneously, thus improving the benzene conversion, xylene selectivity and stability^[125]. Pashkova *et al.* investigated the effects of TPAOH and Na⁺ on aluminum site in zeolite framework during the synthesis of ZSM-5 zeolite^[129]. Yokoi *et al.* also found that in the absence of Na⁺, the aluminum atoms of H-ZSM-5 synthesized by TPA⁺ ions were mainly located at the intersection channels^[130]. In the presence of Na⁺, aluminum atoms existed at the intersection channels, straight channels and sinusoidal channels^[130]. In the ZSM-5 samples prepared with TPA⁺ as the SDA, Al atoms mainly exist at the channel intersection, regardless of the presence or absence of Al pairs [Al-O-(Si-O)₂-Al sequences in one ring]. Adding Na⁺ to the synthetic can only increase the content of Al in the framework (increase the distribution of Al in sinusoidal or straight channels) and adjust the distribution between Al pairs and single isolated Al atoms, but not alter the Al site in the intersection channels.

10-MRS ZEOLITE CHANNELS CYCLE MECHANISM

Double cycle mechanism

It is well known that due to the limitation of ZSM-5 zeolite channels, the MTO/MTA conversion involves several complex chemical reaction processes and carbon pool mechanisms of different intermediate species. The reactions include C-C coupling, olefins methylation, olefin cracking, hydrogen transfer, cyclization, aromatic methylation and aromatic dealkylation^[131]. Numerous intermediates have been reported in the reaction process. Extensive attention has been paid to the hydrocarbon-pool mechanism. The hydrocarbon-pool species can be detected by using ¹³C MAS-NMR. HexaMB, heptamethylbenzene (heptaMB), and pentaMB cations are larger intermediate species, which cannot be formed in the 10-MRs channels and intersection channels of ZSM-5 or react completely after formation^[132]. Nevertheless, the methyl-substituted cyclic hydrocarbon species including pentaMB, dimethyl cyclopentyl (diMCP) and trimethyl cyclopentyl (triMCP) cations are usually the active intermediates in ZSM-5^[133-136]. In the initial stage of MTO reaction, MB is the precursor of light olefins, which can promote the formation of ethylene and propylene. MB and carbocation act together to form propylene through the paring route, which involves the 6↔5-MRs contraction/expansion process^[137].

Numerous studies have been conducted to explore the double cycle mechanisms^[138-141]. The schematic diagram of the double cycle mechanism is shown in Figure 10. Some researchers report that straight channels and sinusoidal channels of ZSM-5 are favorable for the olefin cycle, while the intersection channels are larger than straight/sinusoidal channels and more beneficial for the aromatic cycle^[127,133]. MTH is a self-catalyzed reaction that requires an induction period before reaching a steady state (the formation of hydrocarbon-pool). Hydrocarbon-pool species have a great impact on the reaction route. ZSM-5 displays good reactivity by promoting the double cycle mechanisms of aromatic cycle and olefin cycle. Hydrocarbons, cyclopentenyl cations and MBs are converted to light olefins. Among them, cyclopentene cations are favorable for propylene production, while light MBs such as xylene and triMB are beneficial for ethylene production^[142]. Some researchers consider that pentaMB and hexaMB exist in zeolite channels, but they are hard to react with. Ethylene may be formed through the aromatic carbon pools of lower MBs, while propylene and other high-carbon olefin are formed mainly through olefin methylation and mutual conversion^[132,139,143]. During the reaction, the intermediate species of cycloolefins (cyclopentene, cyclohexene) play a vital role in the aromatization of the olefins^[144]. However, the balance of the double cycle mechanism may be changed by controlling the contact time between methanol and ZSM-5. A low concentration of methanol and a long contact time are favorable for the hydrogen transfer reaction to generate olefin products, thereby further promoting the formation and accumulation of aromatics and

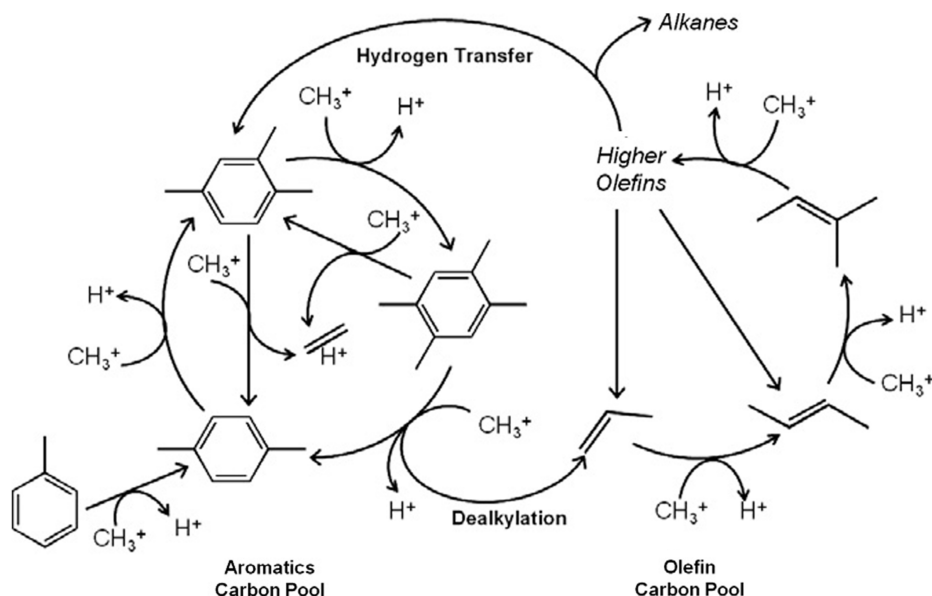


Figure 10. Schematic diagram of dual olefin and aromatic methylation catalytic cycle for methanol to hydrocarbons on H-ZSM-5. The figure is used with permission from Elsevier^[138].

methylcyclopentadiene (MCPs). However, a higher space velocity and a shorter contact time lower the degree of transfer reaction, limit the accumulation of MCPs and aromatics, and eventually promote the formation of propylene or high-carbon olefin^[140].

Three cycle mechanism

In recent years, researchers have proposed that the MTH reaction follows three cycle mechanisms, including olefin cycle, aromatic cycle and aldol cycle^[144,145]. The intermediate species of alcohol-aldehyde cycle mainly include ethanol, acetaldehyde, acetic acid, acetone, methyl acetate, surface methoxyl species and other cyclic oxygenates^[31,146-150]. Aldol is the initial intermediate generated by the reaction from methanol to hydrocarbons on ZSM-5^[151,152]. Cyclic oxygenates undergo the intramolecular aldol cyclization reaction. These polycarbonaceous oxygenate species form the aldol cycle through hydrogen transfer, dehydrogenation, cyclization and cracking. Cyclic oxygenated compounds (such as phenolic compounds) are alkylated to form a series of aromatics species, thus completing the aromatics cycle. Alkenes can also be formed by cracking/decarboxylation of aldol products and/or dealkylation of aromatics^[144].

Acid sites make an impact on the three cycling mechanisms, thereby affecting the distribution of active intermediate species and products. Due to self-condensation and cross-condensations of acetaldehyde and acetone, the chain or cyclic unsaturated aldehydes/ketones were formed. Unsaturated ketones can be converted into alkenes and acetic acid/acetaldehyde is released again to induce the first aldehyde cycle. Meanwhile, the coupling products can be converted into aromatics by hydrogen transfer, cyclization or dehydration, thereby forming the aromatics cycle^[33].

CONCLUSIONS AND OUTLOOK

MFI zeolite with uniform pore size, adjustable acidity and high-temperature resistance displays a broad application prospect. Over the past few decades, zeolite has been an important material for catalytic research due to its shape selectivity. The micropore channels of MFI zeolite are the main place for the entry and exit of reactants or product molecules in the catalytic reaction process. When these molecules diffuse along

different channels in the zeolite crystal, it will lead to the significantly different transmission rates of different channels and the diffusion rates of guest molecules, a phenomenon called “shape selectivity of zeolite”. In addition, the size of single crystal zeolite, the length of b-axis, the active sites and other factors significantly affect the catalytic performance of MFI zeolite. Interestingly, small molecules, such as CO, CO₂, H₂, CH₄, and CH₃OH, can diffuse freely in all microporous channels of the zeolite, and the slight size difference between straight and sinusoidal channels of 10-MRs can regulate the distribution of aromatic products including PX and MX. The larger intersection of straight and sinusoidal channels can facilitate the accommodation of heavy aromatic or polycyclic aromatic intermediates, thereby forming a hydrocarbon pool for catalytic reactions. Based on the above points which have been carefully discussed in the manuscript and in view of the current study on zeolite materials and catalysis, future studies are suggested to concentrate on the following aspects to realize some meaningful achievements:

(i) From the perspective of zeolite channels, the shape selectivity of ZSM-5 zeolite is applicable for the formation of PX. However, the zeolite framework is not a static rigid structure, and the pore size changes due to the vibration of reaction temperature; thus, MX is generated and the selectivity of PX is decreased. Therefore, it is necessary to expose a single crystal plane of the synthesized zeolite to improve the selectivity of a product.

(ii) The regulation of metal active sites via zeolite encapsulation inhibits its growth, but it is difficult to adjust the position of metal encapsulation in zeolite and the size of metal particles. Therefore, how to encapsulate metals specifically in straight channels, sinusoidal channels, at the intersections or in 5/6-MRs is also a topic worthy of in-depth study.

(iii) Up to the present, Al position control (straight channels, sinusoidal channels or intersection) and Al pair control can only be adjusted in a small range. In this regard, it is vital to find a more effective method to locate Al by controlling synthesis conditions or developing new templates. Moreover, the atomic numbers of Al and Si are close, and it is challenging to distinguish and characterize the positions of Al and Si in the ZSM-5 zeolite framework. Although Co(II) UV-vis-DRS analysis is mainly adopted, this method can be subjective and not accurate, and thus it is urgently needed to develop a novel method to determine the Al site.

(iv) Catalytic reactions with zeolite as a catalyst, such as MTA, and MTH, have complex product distribution. Therefore, it is necessary to prepare a catalyst with high selectivity for controllable products.

(v) Due to the complexity of C1 catalytic reaction process, other approaches, including but not limited to the detection of intermediates, are more conducive to further understanding of the entire reaction pathway.

DECLARATIONS

Authors' contributions

Prepared the manuscript: Zhang L, Wang N

Corrected the manuscript: Liu N, Dai C, Xu R, Yu G, Chen B

Availability of data and materials

Not applicable.

Financial support and sponsorship

This research was supported by the National Natural Science Foundation of China (No.22176006, 22178011, 22278008).

Conflicts of interest

All authors declared that there are no conflicts of interest.

Ethical approval and consent to participate

Not applicable.

Consent for publication

Not applicable.

Copyright

© The Author(s) 2023.

REFERENCES

1. Liu C, Us lamin EA, Khramenkova E, et al. High stability of methanol to aromatic conversion over bimetallic Ca,Ga-modified ZSM-5. *ACS Catal* 2022;12:3189-200. DOI PubMed PMC
2. Pfech J, Strossi Pedrolo DR, Marcilio NR, et al. Core-shell metal zeolite composite catalysts for in situ processing of fischer-tropsch hydrocarbons to gasoline type fuels. *ACS Catal* 2020;10:2544-55. DOI
3. Wang X, Zeng C, Gong N, et al. Effective suppression of CO selectivity for CO₂ hydrogenation to high-quality gasoline. *ACS Catal* 2021;11:1528-47. DOI
4. Zuo J, Liu C, Han X, et al. Steering CO₂ hydrogenation coupled with benzene alkylation toward ethylbenzene and propylbenzene using a dual-bed catalyst system. *Chem Catalysis* 2022;2:1223-40. DOI
5. Shen X, Kang J, Niu W, Wang M, Zhang Q, Wang Y. Impact of hierarchical pore structure on the catalytic performances of MFI zeolites modified by ZnO for the conversion of methanol to aromatics. *Catal Sci Technol* 2017;7:3598-612. DOI
6. Wang N, Hou Y, Sun W, et al. Modulation of b-axis thickness within MFI zeolite: correlation with variation of product diffusion and coke distribution in the methanol-to-hydrocarbons conversion. *Appl Catal B-Environ* 2019;243:721-33. DOI
7. Derouane E. A novel effect of shape selectivity: Molecular traffic control in zeolite ZSM-5. *J Catal* 1980;65:486-9. DOI
8. Zeng S, Xu S, Gao S, et al. Differentiating diffusivity in different channels of ZSM-5 zeolite by pulsed field gradient (PFG) NMR. *ChemCatChem* 2020;12:463-8. DOI
9. Cnudde P, De Wispelaere K, Vanduyfhuys L, et al. How chain length and branching influence the alkene cracking reactivity on H-ZSM-5. *ACS Catal* 2018;8:9579-95. DOI PubMed PMC
10. Xu Y, Ma G, Bai J, Du Y, Qin C, Ding M. Yolk@Shell FeMn@Hollow HZSM-5 nanoreactor for directly converting syngas to aromatics. *ACS Catal* 2021;11:4476-85. DOI
11. Liu C, Su J, Liu S, et al. Insights into the key factor of zeolite morphology on the selective conversion of syngas to light aromatics over a Cr₂O₃/ZSM-5 catalyst. *ACS Catal* 2020;10:15227-37. DOI
12. Wang Y, Tan L, Tan M, et al. Rationally designing bifunctional catalysts as an efficient strategy to boost CO₂ hydrogenation producing value-added aromatics. *ACS Catal* 2019;9:895-901. DOI
13. Wang Y, Kazumi S, Gao W, et al. Direct conversion of CO₂ to aromatics with high yield via a modified Fischer-Tropsch synthesis pathway. *Appl Catal B-Environ* 2020;269:118792. DOI
14. Wang T, Xu Y, Li Y, et al. Sodium-mediated bimetallic Fe-Ni catalyst boosts stable and selective production of light aromatics over HZSM-5 zeolite. *ACS Catal* 2021;11:3553-74. DOI
15. Liao Y, Zhong R, Makshina E, et al. Propylphenol to phenol and propylene over acidic zeolites: role of shape selectivity and presence of steam. *ACS Catal* 2018;8:7861-78. DOI
16. Li J, Gong Q, Lian H, Hu Z, Zhu Z. New process for 2,6-dimethylnaphthalene synthesis by using C₁₀ aromatics as solvent and transmethylation-agentia: high-efficiency and peculiar subarea-catalysis over shape-selective ZSM-5/Beta catalyst. *Ind Eng Chem Res* 2019;58:12593-601. DOI
17. Liu F, Willhammar T, Wang L, et al. ZSM-5 zeolite single crystals with b-axis-aligned mesoporous channels as an efficient catalyst for conversion of bulky organic molecules. *J Am Chem Soc* 2012;134:4557-60. DOI PubMed
18. Ali B, Lan X, Arslan MT, Gilani SZA, Wang H, Wang T. Controlling the selectivity and deactivation of H-ZSM-5 by tuning b-axis channel length for glycerol dehydration to acrolein. *J Ind Eng Chem* 2020;88:127-36. DOI
19. Zhang J, Ren L, Zhou A, et al. Tailored synthesis of ZSM-5 nanosheets with controllable. *b* ;34:3217-26. DOI
20. Ye J, Bai L, Liu B, et al. Fabrication of a pillared ZSM-5 framework for shape selectivity of ethane dehydroaromatization. *Ind Eng*

- Chem Res* 2019;58:7094-106. [DOI](#)
21. Ma Z, Fu T, Wang Y, et al. Silicalite-1 derivational desilication-recrystallization to prepare hollow Nano-ZSM-5 and Highly mesoporous micro-ZSM-5 catalyst for methanol to hydrocarbons. *Ind Eng Chem Res* 2019;58:2146-58. [DOI](#)
 22. Xu Y, Wang J, Ma G, Lin J, Ding M. Designing of hollow ZSM-5 with controlled mesopore sizes to boost gasoline production from syngas. *ACS Sustainable Chem Eng* 2019;7:18125-32. [DOI](#)
 23. Zhang H, Song K, Wang L, Zhang H, Zhang Y, Tang Y. Organic structure directing agent-free and seed-induced synthesis of enriched intracrystal mesoporous ZSM-5 zeolite for shape-selective reaction. *ChemCatChem* 2013;5:2874-8. [DOI](#)
 24. Kang J, Cheng K, Zhang L, et al. Mesoporous zeolite-supported ruthenium nanoparticles as highly selective Fischer-Tropsch catalysts for the production of C₅-C₁₁ isoparaffins. *Angew Chem Int Ed Engl* 2011;50:5200-3. [DOI](#) [PubMed](#)
 25. Knott BC, Nimlos CT, Robichaud DJ, Nimlos MR, Kim S, Gounder R. Consideration of the aluminum distribution in zeolites in theoretical and experimental catalysis research. *ACS Catal* 2018;8:770-84. [DOI](#)
 26. Sharada S, Zimmerman PM, Bell AT, Head-gordon M. Insights into the kinetics of cracking and dehydrogenation reactions of light alkanes in H-MFI. *J Phys Chem C* 2013;117:12600-11. [DOI](#)
 27. Wang S, Li Z, Qin Z, et al. Catalytic roles of the acid sites in different pore channels of H-ZSM-5 zeolite for methanol-to-olefins conversion. *Chinese J Catal* 2021;42:1126-36. [DOI](#)
 28. Sun Q, Wang N, Fan Q, et al. Subnanometer bimetallic platinum-zinc clusters in zeolites for propane dehydrogenation. *Angewandte Chemie* 2020;132:19618-27. [DOI](#) [PubMed](#)
 29. Sun Q, Chen BWJ, Wang N, et al. Zeolite-encaged Pd-Mn nanocatalysts for CO₂ hydrogenation and formic acid dehydrogenation. *Angew Chem Int Ed Engl* 2020;59:20183-91. [DOI](#) [PubMed](#)
 30. Liu L, Lopez-Haro M, Lopes CW, et al. Regioselective generation and reactivity control of subnanometric platinum clusters in zeolites for high-temperature catalysis. *Nat Mater* 2019;18:866-73. [DOI](#) [PubMed](#)
 31. Yang L, Yan T, Wang C, et al. Role of acetaldehyde in the roadmap from initial carbon-carbon bonds to hydrocarbons during methanol conversion. *ACS Catal* 2019;9:6491-501. [DOI](#)
 32. Fu D, Maris JJE, Stanciakova K, et al. Unravelling channel structure-diffusivity relationships in zeolite ZSM-5 at the single-molecule level. *Angewandte Chemie* 2022:134. [DOI](#) [PubMed](#) [PMC](#)
 33. Yang L, Wang C, Dai W, Wu G, Guan N, Li L. Progressive steps and catalytic cycles in methanol-to-hydrocarbons reaction over acidic zeolites. *Fundamental Res* 2022;2:184-92. [DOI](#)
 34. Gobin O, Reitmeier S, Jentys A, Lercher J. Diffusion pathways of benzene, toluene and p-xylene in MFI. *Microporous Mesoporous Mater* 2009;125:3-10. [DOI](#)
 35. Deluca M, Hibbitts D. Predicting diffusion barriers and diffusivities of C₆-C₁₂ methylbenzenes in MFI zeolites. *Microporous Mesoporous Mater* 2022;333:111705. [DOI](#)
 36. Baumgärtl M, Jentys A, Lercher JA. Understanding elementary steps of transport of xylene mixtures in ZSM-5 zeolites. *J Phys Chem C* 2019;123:8092-100. [DOI](#)
 37. Kubarev AV, Breynaert E, Van Loon J, et al. Solvent polarity-induced pore selectivity in H-ZSM-5 catalysis. *ACS Catal* 2017;7:4248-52. [DOI](#) [PubMed](#) [PMC](#)
 38. Liu C, Su J, Xiao Y, et al. Constructing directional component distribution in a bifunctional catalyst to boost the tandem reaction of syngas conversion. *Chem Catalysis* 2021;1:896-907. [DOI](#)
 39. Korde A, Min B, Kapaca E, et al. Single-walled zeolitic nanotubes. *Science* 2022;375:62-6. [DOI](#) [PubMed](#)
 40. Jeon MY, Kim D, Kumar P, et al. Ultra-selective high-flux membranes from directly synthesized zeolite nanosheets. *Nature* 2017;543:690-4. [DOI](#) [PubMed](#)
 41. Choi M, Na K, Kim J, Sakamoto Y, Terasaki O, Ryoo R. Stable single-unit-cell nanosheets of zeolite MFI as active and long-lived catalysts. *Nature* 2009;461:246-9. [DOI](#) [PubMed](#)
 42. Xiao X, Zhang Y, Jiang G, et al. Simultaneous realization of high catalytic activity and stability for catalytic cracking of n-heptane on highly exposed (010) crystal planes of nanosheet ZSM-5 zeolite. *Chem Commun (Camb)* 2016;52:10068-71. [DOI](#) [PubMed](#)
 43. Qureshi BA, Lan X, Arslan MT, Wang T. Highly active and selective nano H-ZSM-5 catalyst with short channels along. *Ind Eng Chem Res* 2019;58:12611-22. [DOI](#)
 44. Mohammadparast F, Halladj R, Askari S. The crystal size effect of nano-sized ZSM-5 in the catalytic performance of petrochemical processes: a review. *Chem Eng Commun* 2015;202:542-56. [DOI](#)
 45. Ma Y, Cai D, Li Y, et al. The influence of straight pore blockage on the selectivity of methanol to aromatics in nanosized Zn/ZSM-5: an atomic Cs-corrected STEM analysis study. *RSC Adv* 2016;6:74797-801. [DOI](#)
 46. Kim J, Kim W, Seo Y, Kim J, Ryoo R. n-Heptane hydroisomerization over Pt/MFI zeolite nanosheets: effects of zeolite crystal thickness and platinum location. *J Catal* 2013;301:187-97. [DOI](#)
 47. Ma Y, Wang N, Qian W, Wang Y, Zhang J, Wei F. Molded MFI nanocrystals as a highly active catalyst in a methanol-to-aromatics process. *RSC Adv* 2016;6:81198-202. [DOI](#)
 48. Ma X, Li G, Tao J, et al. Synergistic chemical synthesis and self-assembly lead to three-dimensional b-oriented MFI superstructures with selective adsorption and luminescence properties. *Chemistry* 2018;24:2980-6. [DOI](#) [PubMed](#)
 49. Liu Y, Zhou X, Pang X, et al. Improved para-xylene selectivity in meta-xylene isomerization over ZSM-5 crystals with relatively long b-axis length. *ChemCatChem* 2013;5:1517-23. [DOI](#)
 50. Wang T, Yang C, Gao P, et al. ZnZrOx integrated with chain-like nanocrystal HZSM-5 as efficient catalysts for aromatics synthesis

- from CO₂ hydrogenation. *Appl Catal B-Environ* 2021;286:119929. DOI
51. Yang J, Gong K, Miao D, et al. Enhanced aromatic selectivity by the sheet-like ZSM-5 in syngas conversion. *J Energy Chem* 2019;35:44-8. DOI
 52. Wang N, Sun W, Hou Y, et al. Crystal-plane effects of MFI zeolite in catalytic conversion of methanol to hydrocarbons. *J Catal* 2018;360:89-96. DOI
 53. Wang C, Zhang L, Huang X, et al. Maximizing sinusoidal channels of HZSM-5 for high shape-selectivity to p-xylene. *Nat Commun* 2019;10:4348. DOI PubMed PMC
 54. Miao L, Hong Z, Zhao G, Huang F, Zhu Z. Mo-Modified ZSM-5 zeolite with intergrowth crystals for high-efficiency catalytic xylene isomerization. *Catal Sci Technol* 2021;11:4831-7. DOI
 55. Chen Q, Liu J, Yang B. Identifying the key steps determining the selectivity of toluene methylation with methanol over HZSM-5. *Nat Commun* 2021;12:3725. DOI PubMed PMC
 56. Cai D, Wang N, Chen X, et al. Highly selective conversion of methanol to propylene: design of an MFI zeolite with selective blockage of (010) surfaces. *Nanoscale* 2019;11:8096-101. DOI PubMed
 57. Bonilla G, Díaz I, Tsapatsis M, Jeong H, Lee Y, Vlachos DG. Zeolite (MFI) crystal morphology control using organic structure-directing agents. *Chem Mater* 2004;16:5697-705. DOI
 58. Kim E, Choi J, Tsapatsis M. On defects in highly a-oriented MFI membranes. *Microporous Mesoporous Mater* 2013;170:1-8. DOI
 59. Lai Z, Bonilla G, Diaz I, et al. Microstructural optimization of a zeolite membrane for organic vapor separation. *Science* 2003;300:456-60. DOI PubMed
 60. Choi J, Ghosh S, King L, Tsapatsis M. MFI zeolite membranes from a- and randomly oriented monolayers. *Adsorption* 2006;12:339-60. DOI
 61. Pham TCT, Kim HS, Yoon KB. Growth of uniformly oriented silica MFI and BEA zeolite films on substrates. *Science* 2011;334:1533-8. DOI PubMed
 62. Danilina N, Krumeich F, Castelanelli SA, van Bokhoven JA. Where are the active sites in zeolites? *J Phys Chem C* 2010;114:6640-5. DOI
 63. Zuo J, Chen W, Liu J, Duan X, Ye L, Yuan Y. Selective methylation of toluene using CO₂ and H₂ to para-xylene. *Sci Adv* 2020;6. DOI PubMed PMC
 64. Zhang P, Tan L, Yang G, Tsubaki N. One-pass selective conversion of syngas to para-xylene. *Chem Sci* 2017;8:7941-6. DOI PubMed PMC
 65. Gao W, Guo L, Wu Q, et al. Capsule-like zeolite catalyst fabricated by solvent-free strategy for para-Xylene formation from CO₂ hydrogenation. *Appl Catal B-Environ* 2022;303:120906. DOI
 66. Wang N, Li J, Sun W, et al. Rational design of Zinc/Zeolite catalyst: selective formation of p-Xylene from methanol to aromatics reaction. *Angew Chem Int Ed Engl* 2022;61:e202114786. DOI PubMed
 67. Sun Q, Wang N, Yu J. Advances in catalytic applications of zeolite-supported metal catalysts. *Adv Mater* 2021;33:e2104442. DOI PubMed
 68. Wang N, Sun Q, Yu J. Ultrasmall metal nanoparticles confined within crystalline nanoporous materials: a fascinating class of nanocatalysts. *Adv Mater* 2019;31:e1803966. DOI PubMed
 69. Chai Y, Shang W, Li W, et al. Noble metal particles confined in zeolites: synthesis, characterization, and applications. *Adv Sci (Weinh)* 2019;6:1900299. DOI PubMed PMC
 70. Ou Z, Li Y, Wu W, et al. Encapsulating subnanometric metal clusters in zeolites for catalysis and their challenges. *Chem Eng J* 2022;430:132925. DOI
 71. Wang N, Sun Q, Zhang T, et al. Impregnating subnanometer metallic nanocatalysts into self-pillared zeolite nanosheets. *J Am Chem Soc* 2021;143:6905-14. DOI PubMed
 72. Iida T, Zanchet D, Ohara K, Wakihara T, Román-leshkov Y. Concerted bimetallic nanocluster synthesis and encapsulation via induced zeolite framework demetallation for shape and substrate selective heterogeneous catalysis. *Angew Chem* 2018;130:6564-8. DOI PubMed
 73. den Broek A, van Grondelle J, van Santen R. Preparation of highly dispersed platinum particles in hzsm-5 zeolite: a study of the pretreatment process of [Pt(NH₃)₄]²⁺. *J Catal* 1997;167:417-24. DOI
 74. Wang N, Sun Q, Bai R, Li X, Guo G, Yu J. In situ confinement of ultrasmall pd clusters within nanosized silicalite-I zeolite for highly efficient catalysis of hydrogen generation. *J Am Chem Soc* 2016;138:7484-7. DOI PubMed
 75. Sun Q, Wang N, Bing Q, et al. Subnanometric hybrid Pd-M(OH)₂, M = Ni, Co, clusters in zeolites as highly efficient nanocatalysts for hydrogen generation. *Chem* 2017;3:477-93. DOI
 76. Mielby J, Abildstrøm JO, Wang F, Kasama T, Weidenthaler C, Kegnaes S. Oxidation of bioethanol using zeolite-encapsulated gold nanoparticles. *Angew Chem* 2014;126:12721-4. DOI PubMed
 77. Kurbanova A, Zákutná D, Gołabek K, Mazur M, Přeč J. Preparation of Fe@MFI and CuFe@MFI composite hydrogenation catalysts by reductive demetallation of Fe-zeolites. *Catal Today* 2022;390-391:306-15. DOI
 78. Zhu J, Osuga R, Ishikawa R, et al. Ultrafast encapsulation of metal nanoclusters into MFI zeolite in the course of its crystallization: catalytic application for propane dehydrogenation. *Angew Chem Int Ed Engl* 2020;59:19669-74. DOI PubMed
 79. Oda A, Torigoe H, Itadani A, et al. Success in making Zn⁺ from atomic Zn⁰ encapsulated in an MFI-type zeolite with UV light irradiation. *J Am Chem Soc* 2013;135:18481-9. DOI PubMed

80. Goel S, Zones SI, Iglesia E. Encapsulation of metal clusters within MFI via interzeolite transformations and direct hydrothermal syntheses and catalytic consequences of their confinement. *J Am Chem Soc* 2014;136:15280-90. [DOI](#) [PubMed](#)
81. Zhang Y, Li A, Sajad M, et al. Imidazolium-type ionic liquid-assisted formation of the MFI zeolite loaded with metal nanoparticles for hydrogenation reactions. *Chem Eng J* 2021;412:128599. [DOI](#)
82. Yang J, He Y, He J, et al. Enhanced catalytic performance through in situ encapsulation of ultrafine ru clusters within a high-aluminum zeolite. *ACS Catal* 2022;12:1847-56. [DOI](#)
83. Gu J, Zhang Z, Hu P, et al. Platinum nanoparticles encapsulated in MFI Zeolite crystals by a two-step dry gel conversion method as a highly selective hydrogenation catalyst. *ACS Catal* 2015;5:6893-901. [DOI](#)
84. Sun Q, Wang N, Zhang T, et al. Zeolite-encaged single-atom rhodium catalysts: highly-efficient hydrogen generation and shape-selective tandem hydrogenation of nitroarenes. *Angew Chem Int Ed Engl* 2019;58:18570-6. [DOI](#) [PubMed](#)
85. Li T, Beck A, Krumeich F, et al. Stable palladium oxide clusters encapsulated in silicalite-1 for complete methane oxidation. *ACS Catal* 2021;11:7371-82. [DOI](#)
86. Liu L, Lopez-haro M, Lopes CW, et al. Atomic-level understanding on the evolution behavior of subnanometric Pt and Sn species during high-temperature treatments for generation of dense PtSn clusters in zeolites. *J Catal* 2020;391:11-24. [DOI](#)
87. Wang N, Qian W, Shen K, Su C, Wei F. Bayberry-like ZnO/MFI zeolite as high performance methanol-to-aromatics catalyst. *Chem Commun (Camb)* 2016;52:2011-4. [DOI](#) [PubMed](#)
88. Wang Q, Xu S, Chen J, et al. Synthesis of mesoporous ZSM-5 catalysts using different mesogenous templates and their application in methanol conversion for enhanced catalyst lifespan. *RSC Adv* 2014;4:21479-91. [DOI](#)
89. Zhou J, Hua Z, Liu Z, Wu W, Zhu Y, Shi J. Direct synthetic strategy of mesoporous ZSM-5 zeolites by using conventional block copolymer templates and the improved catalytic properties. *ACS Catal* 2011;1:287-91. [DOI](#)
90. Liu B, Li C, Ren Y, Tan Y, Xi H, Qian Y. Direct synthesis of mesoporous ZSM-5 zeolite by a dual-functional surfactant approach. *Chem Eng J* 2012;210:96-102. [DOI](#)
91. Zhou J, Hua Z, Wu W, et al. Hollow mesoporous zeolite microspheres: hierarchical macro-/meso-/microporous structure and exceptionally enhanced adsorption properties. *Dalton Trans* 2011;40:12667-9. [DOI](#) [PubMed](#)
92. Chen G, Li J, Wang S, et al. Construction of Single-Crystalline Hierarchical ZSM-5 with Open Nanoarchitectures via Anisotropic-Kinetics Transformation for the Methanol-to-Hydrocarbons Reaction. *Angew Chem Int Ed Engl* 2022;61:e202200677. [DOI](#) [PubMed](#)
93. Ogura M, Shinomiya S, Tateno J, et al. Alkali-treatment technique-new method for modification of structural and acid-catalytic properties of ZSM-5 zeolites. *APPL CATAL A-GEN* 2001;219:33-43. [DOI](#)
94. Groen JC, Bach T, Ziese U, et al. Creation of hollow zeolite architectures by controlled desilication of Al-zoned ZSM-5 crystals. *J Am Chem Soc* 2005;127:10792-3. [DOI](#) [PubMed](#)
95. Dong A, Ren N, Yang W, et al. Preparation of hollow zeolite spheres and three-dimensionally ordered macroporous zeolite monoliths with functionalized interiors. *Adv Funct Mater* 2003;13:943-8. [DOI](#)
96. Liu Y, Qiang W, Ji T, et al. Uniform hierarchical MFI nanosheets prepared via anisotropic etching for solution-based sub-100-nm-thick oriented MFI layer fabrication. *Sci Adv* 2020;6:eaay5993. [DOI](#) [PubMed](#) [PMC](#)
97. Zhou T, Zhang D, Liu Y, et al. Construction of monodispersed single-crystalline hierarchical ZSM-5 nanosheets via anisotropic etching. *J Energy Chem* 2022;72:516-21. [DOI](#)
98. Han S, Wang Z, Meng L, Jiang N. Synthesis of uniform mesoporous ZSM-5 using hydrophilic carbon as a hard template. *Mater Chem Phys* 2016;177:112-7. [DOI](#)
99. Kim S, Shah J, Pinnavaia TJ. Colloid-imprinted carbons as templates for the nanocasting synthesis of mesoporous ZSM-5 zeolite. *Chem Mater* 2003;15:1664-8. [DOI](#)
100. Chen H, Wang Y, Sun C, Wang X, Wang C. Synthesis of hierarchical ZSM-5 zeolites with CTAB-containing seed silicalite-1 and its catalytic performance in methanol to propylene. *Catal Commun* 2018;112:10-4. [DOI](#)
101. Dai C, Zhang A, Li L, et al. Synthesis of hollow nanocubes and macroporous monoliths of silicalite-1 by alkaline treatment. *Chem Mater* 2013;25:4197-205. [DOI](#)
102. Jin W, Qiao J, Yu J, Wang Y, Cao J. Influence of hollow ZSM-5 zeolites prepared by treatment with different alkalis on the catalytic conversion of methanol to aromatics. *Energy Fuels* 2020;34:14633-46. [DOI](#)
103. Dai C, Zhang A, Liu M, Guo X, Song C. Hollow ZSM-5 with silicon-rich surface, double shells, and functionalized interior with metallic nanoparticles and carbon nanotubes. *Adv Funct Mater* 2015;25:7479-87. [DOI](#)
104. Kwok KM, Ong SWD, Chen L, Zeng HC. Transformation of stober silica spheres to hollow hierarchical single-crystal ZSM-5 zeolites with encapsulated metal nanocatalysts for selective catalysis. *ACS Appl Mater Interfaces* 2019;11:14774-85. [DOI](#) [PubMed](#)
105. Dai C, Zhang A, Song C, Guo X. Advances in the synthesis and catalysis of solid and hollow zeolite-encapsulated metal catalysts. Elsevier; 2018. p. 75-115. [DOI](#)
106. Han SW, Park H, Han J, et al. PtZn intermetallic compound nanoparticles in mesoporous zeolite exhibiting high catalyst durability for propane dehydrogenation. *ACS Catal* 2021;11:9233-41. [DOI](#)
107. Cho HJ, Kim D, Li S, Su D, Ma D, Xu B. Molecular-level proximity of metal and acid sites in zeolite-encapsulated Pt nanoparticles for selective multistep tandem catalysis. *ACS Catal* 2020;10:3340-8. [DOI](#)
108. Rasmussen KH, Goodarzi F, Christensen DB, Mielby J, Kegnæs S. Stabilization of metal nanoparticle catalysts via encapsulation in mesoporous zeolites by steam-assisted recrystallization. *ACS Appl Nano Mater* 2019;2:8083-91. [DOI](#)
109. Peng H, Dong T, Yang S, et al. Intra-crystalline mesoporous zeolite encapsulation-derived thermally robust metal nanocatalyst in

- deep oxidation of light alkanes. *Nat Commun* 2022;13:295. DOI PubMed PMC
110. Chen Y, Zhu X, Wang X, Su Y. A reliable protocol for fast and facile constructing multi-hollow silicalite-1 and encapsulating metal nanoparticles within the hierarchical zeolite. *Chem Eng J* 2021;419:129641. DOI
 111. Gao X, Zhou Y, Feng L, et al. Direct low-temperature hydrothermal synthesis of uniform Pd nanoparticles encapsulated mesoporous TS-1 and its excellent catalytic capability. *Microporous Mesoporous Mater* 2019;283:82-7. DOI
 112. Cui T, Ke W, Zhang W, Wang H, Li X, Chen J. Encapsulating palladium nanoparticles inside mesoporous mfi zeolite nanocrystals for shape-selective catalysis. *Angew Chem* 2016;128:9324-8. DOI PubMed
 113. Thumbayil R, Mielby J, Kegnæs S. Pd Nanoparticles encapsulated in mesoporous HZSM-5 zeolite for selective one-step conversion of acetone to methyl isobutyl ketone. *Top Catal* 2019;62:678-88. DOI
 114. Jia X, Jiang J, Zou S, et al. Library creation Of ultrasmall multi-metallic nanoparticles confined in mesoporous MFI zeolites. *Angew Chem Int Ed Engl* 2021;60:14571-7. DOI PubMed
 115. Dai C, Zhang A, Liu M, Gu L, Guo X, Song C. Hollow alveolus-like nanovesicle assembly with metal-encapsulated hollow zeolite nanocrystals. *ACS Nano* 2016;10:7401-8. DOI PubMed
 116. Shen X, Mao W, Ma Y, et al. A hierarchical MFI zeolite with a two-dimensional square mesostructure. *Angew Chem* 2018;130:732-6. DOI PubMed
 117. Zhang Y, Shen X, Gong Z, Han L, Sun H, Che S. Single-crystalline MFI zeolite with sheet-like mesopores layered along the a axis. *Chemistry* 2019;25:738-42. DOI PubMed
 118. Singh BK, Xu D, Han L, Ding J, Wang Y, Che S. Synthesis of single-crystalline mesoporous ZSM-5 with three-dimensional pores via the self-assembly of a designed triply branched cationic surfactant. *Chem Mater* 2014;26:7183-8. DOI
 119. Kim J, Ryoo R, Opanasenko MV, Shamzhy MV, Čejka J. Mesoporous MFI zeolite nanosponge as a high-performance catalyst in the pechmann condensation reaction. *ACS Catal* 2015;5:2596-604. DOI
 120. Zhang X, Liu D, Xu D, et al. Synthesis of self-pillared zeolite nanosheets by repetitive branching. *Science* 2012;336:1684-7. DOI PubMed
 121. Wang N, Qian W, Wei F. Fabrication and catalytic properties of three-dimensional ordered zeolite arrays with interconnected micro-meso-macroporous structure. *J Mater Chem A* 2016;4:10834-41. DOI
 122. Ghorbanpour A, Rimer JD, Grabow LC. Periodic, vdW-corrected density functional theory investigation of the effect of Al siting in H-ZSM-5 on chemisorption properties and site-specific acidity. *Catal Commun* 2014;52:98-102. DOI
 123. Vankoningsveld H, Jansen J, Vanbekkum H. The monoclinic framework structure of zeolite H-ZSM-5. Comparison with the orthorhombic framework of as-synthesized ZSM-5. *Zeolites* 1990;10:235-42. DOI
 124. Kim S, Park G, Woo MH, Kwak G, Kim SK. Control of hierarchical structure and framework-al distribution of ZSM-5 via adjusting crystallization temperature and their effects on methanol conversion. *ACS Catal* 2019;9:2880-92. DOI
 125. Wang Y, He X, Yang F, Su Z, Zhu X. Control of framework aluminum distribution in MFI channels on the catalytic performance in alkylation of benzene with methanol. *Ind Eng Chem Res* 2020;59:13420-7. DOI
 126. Dědeček J, Sobalík Z, Wichterlová B. Siting and distribution of framework aluminium atoms in silicon-rich zeolites and impact on catalysis. *Catal Rev* 2012;54:135-223. DOI
 127. Liang T, Chen J, Qin Z, et al. Conversion of methanol to olefins over H-ZSM-5 zeolite: reaction pathway is related to the framework aluminum siting. *ACS Catal* 2016;6:7311-25. DOI
 128. Chen K, Wu X, Zhao J, et al. Organic-free modulation of the framework Al distribution in ZSM-5 zeolite by magnesium participated synthesis and its impact on the catalytic cracking reaction of alkanes. *J Catal* 2022;413:735-50. DOI
 129. Pashkova V, Sklenak S, Klein P, Urbanova M, Dědeček J. Location of framework Al atoms in the channels of ZSM-5: effect of the (hydrothermal) synthesis. *Chemistry* 2016;22:3937-41. DOI PubMed
 130. Yokoi T, Mochizuki H, Namba S, Kondo JN, Tatsumi T. Control of the Al distribution in the framework of ZSM-5 zeolite and its evaluation by solid-state NMR technique and catalytic properties. *J Phys Chem C* 2015;119:15303-15. DOI
 131. Ilias S, Bhan A. Mechanism of the catalytic conversion of methanol to hydrocarbons. *ACS Catal* 2013;3:18-31. DOI
 132. Bjørgen M, Svelle S, Joensen F, et al. Conversion of methanol to hydrocarbons over zeolite H-ZSM-5: on the origin of the olefinic species. *J Catal* 2007;249:195-207. DOI
 133. Zhang M, Xu S, Wei Y, et al. Methanol conversion on ZSM-22, ZSM-35 and ZSM-5 zeolites: effects of 10-membered ring zeolite structures on methylcyclopentenyl cations and dual cycle mechanism. *RSC Adv* 2016;6:95855-64. DOI
 134. Haw JF, Nicholas JB, Song W, et al. Roles for cyclopentenyl cations in the synthesis of hydrocarbons from methanol on zeolite catalyst HZSM-5. *J Am Chem Soc* 2000;122:4763-75. DOI
 135. Svelle S, Joensen F, Nerlov J, et al. Conversion of methanol into hydrocarbons over zeolite H-ZSM-5: ethene formation is mechanistically separated from the formation of higher alkenes. *J Am Chem Soc* 2006;128:14770-1. DOI PubMed
 136. Haw JF, Goguen PW, Xu T, Skloss TW, Song W, Wang Z. In situ NMR investigations of heterogeneous catalysis with samples prepared under standard reaction conditions. *Angew Chem Int Ed* 1998;37:948-9. DOI PubMed
 137. Wang C, Chu Y, Zheng A, et al. Frontispiece: new insight into the hydrocarbon-pool chemistry of the methanol-to-olefins conversion over zeolite H-ZSM-5 from GC-MS, solid-state NMR spectroscopy, and DFT calculations. *Chem Eur J* 2014;20:12432-43. DOI
 138. Ilias S, Bhan A. Tuning the selectivity of methanol-to-hydrocarbons conversion on H-ZSM-5 by co-processing olefin or aromatic compounds. *J Catal* 2012;290:186-92. DOI
 139. Bjørgen M, Joensen F, Lillerud K, Olsbye U, Svelle S. The mechanisms of ethene and propene formation from methanol over high

- silica H-ZSM-5 and H-beta. *Catal Today* 2009;142:90-7. DOI
140. Zhang M, Xu S, Wei Y, et al. Changing the balance of the MTO reaction dual-cycle mechanism: Reactions over ZSM-5 with varying contact times. *Chinese J Catal* 2016;37:1413-22. DOI
 141. Dai W, Yang L, Wang C, et al. Effect of n -butanol cofeeding on the methanol to aromatics conversion over ga-modified nano H-ZSM-5 and its mechanistic interpretation. *ACS Catal* ;8:1352-62. DOI
 142. Wang C, Sun X, Xu J, et al. Impact of temporal and spatial distribution of hydrocarbon pool on methanol conversion over H-ZSM-5. *J Catal* 2017;354:138-51. DOI
 143. Gao P, Xu J, Qi G, et al. A mechanistic study of methanol-to-aromatics reaction over Ga-modified ZSM-5 zeolites: understanding the dehydrogenation process. *ACS Catal* 2018;8:9809-20. DOI
 144. Arslan MT, Ali B, Gilani SZA, et al. Selective conversion of syngas into tetramethylbenzene via an aldol-aromatic mechanism. *ACS Catal* 2020;10:2477-88. DOI
 145. Arslan MT, Tian G, Ali B, et al. Highly selective conversion of CO₂ or CO into precursors for kerosene-based aviation fuel via an aldol-aromatic mechanism. *ACS Catal* 2022;12:2023-33. DOI
 146. Comas-Vives A, Valla M, Copéret C, Sautet P. Cooperativity between Al sites promotes hydrogen transfer and carbon-carbon bond formation upon dimethyl ether activation on alumina. *ACS Cent Sci* 2015;1:313-9. DOI PubMed PMC
 147. Liu Y, Müller S, Berger D, et al. Formation mechanism of the first carbon-carbon bond and the first olefin in the methanol conversion into hydrocarbons. *Angew Chem* 2016;128:5817-20. DOI
 148. Wu X, Xu S, Zhang W, et al. Direct mechanism of the first carbon-carbon bond formation in the methanol-to-hydrocarbons process. *Angew Chem* 2017;129:9167-71. DOI PubMed
 149. Wang C, Chu Y, Xu J, et al. Extra-framework aluminum-assisted initial C-C bond formation in methanol-to-olefins conversion on zeolite H-ZSM-5. *Angew Chem* 2018;130:10354-8. DOI PubMed
 150. Ni Y, Zhu W, Liu Z. H-ZSM-5-catalyzed hydroacylation involved in the coupling of methanol and formaldehyde to aromatics. *ACS Catal* 2019;9:11398-403. DOI
 151. Liu Y, Kirchberger FM, Müller S, et al. Critical role of formaldehyde during methanol conversion to hydrocarbons. *Nat Commun* 2019;10:1462. DOI PubMed PMC
 152. Chen Z, Ni Y, Zhi Y, et al. Coupling of methanol and carbon monoxide over H-ZSM-5 to form aromatics. *Angew Chem Int Ed Engl* 2018;57:12549-53. DOI PubMed